



IFN-Stimulated Gene 15 Is an Alarmin that Boosts the CTL Response via an Innate, NK Cell-Dependent Route

This information is current as of May 5, 2020.

Victoria Iglesias-Guimaraes, Tomasz Ahrends, Evert de Vries, Klaus-Peter Knobloch, Andriy Volkov and Jannie Borst

J Immunol 2020; 204:2110-2121; Prepublished online 13 March 2020;
doi: 10.4049/jimmunol.1901410
<http://www.jimmunol.org/content/204/8/2110>

Supplementary Material <http://www.jimmunol.org/content/suppl/2020/03/12/jimmunol.1901410.DCSupplemental>

References This article **cites 61 articles**, 28 of which you can access for free at:
<http://www.jimmunol.org/content/204/8/2110.full#ref-list-1>

Why *The JI*? Submit online.

- **Rapid Reviews! 30 days*** from submission to initial decision
- **No Triage!** Every submission reviewed by practicing scientists
- **Fast Publication!** 4 weeks from acceptance to publication

**average*

Subscription Information about subscribing to *The Journal of Immunology* is online at:
<http://jimmunol.org/subscription>

Permissions Submit copyright permission requests at:
<http://www.aai.org/About/Publications/JI/copyright.html>

Author Choice Freely available online through *The Journal of Immunology*
[Author Choice option](#)

Email Alerts Receive free email-alerts when new articles cite this article. Sign up at:
<http://jimmunol.org/alerts>

IFN-Stimulated Gene 15 Is an Alarmin that Boosts the CTL Response via an Innate, NK Cell–Dependent Route

Victoria Iglesias-Guimaraes,* Tomasz Ahrends,*¹ Evert de Vries,*^{†,‡}
Klaus-Peter Knobeloch,[§] Andriy Volkov,* and Jannie Borst*^{†,‡}

Type I IFN is produced upon infection and tissue damage and induces the expression of many IFN-stimulated genes (ISGs) that encode host-protective proteins. ISG15 is a ubiquitin-like molecule that can be conjugated to proteins but is also released from cells in a free form. Free, extracellular ISG15 is suggested to have an immune-regulatory role, based on disease phenotypes of ISG15-deficient humans and mice. However, the underlying mechanisms by which free ISG15 would act as a “cytokine” are unclear and much debated. We, in this study, demonstrate in a clinically relevant mouse model of therapeutic vaccination that free ISG15 is an alarmin that induces tissue alert, characterized by extracellular matrix remodeling, myeloid cell infiltration, and inflammation. Moreover, free ISG15 is a potent adjuvant for the CTL response. ISG15 produced at the vaccination site promoted the vaccine-specific CTL response by enhancing expansion, short-lived effector and effector/memory differentiation of CD8⁺ T cells. The function of free ISG15 as an extracellular ligand was demonstrated, because the equivalents in murine ISG15 of 2 aa recently implicated in binding of human ISG15 to LFA-1 *in vitro* were required for its adjuvant effect *in vivo*. Moreover, in further agreement with the *in vitro* findings on human cells, free ISG15 boosted the CTL response *in vivo* via NK cells in the absence of CD4⁺ T cell help. Thus, free ISG15 is part of a newly recognized innate route to promote the CTL response. *The Journal of Immunology*, 2020, 204: 2110–2121.

Infection and tissue damage lead to the production of type I IFNs (IFN-I). These cytokines induce the expression of many IFN-stimulated genes (ISGs), encoding proteins that

protect the host in many different ways (1). This group of proteins includes ISG15 that has a diubiquitin-like structure (2). *Isg15* is one of the genes most strongly upregulated in response to viral infection in a diversity of species, including humans (3, 4). ISG15 is also induced by bacterial infections (5, 6). *Isg15*-deficient mice and humans display phenotypes that indicate a role for ISG15 in the protection against infection, but the underlying mechanisms have not been fully elucidated (3, 7, 8). ISG15 can be conjugated to proteins but also exists in a free form and thus may act by different mechanisms either within or outside the cell.

Like ubiquitin, ISG15 can be covalently conjugated to lysine residues through a C-terminal diglycine motif (LRLRGG) (9). This process, termed ISGylation, relies on one E1-activating enzyme (UBE1L) (10), one E2 enzyme (UBC8) (11, 12), and one major E3 enzyme (HERC5 in humans and HERC6 in mice) (13, 14). ISGylation is reversible, and the major ISG15-deconjugating enzyme *in vivo* is USP18/UBP43 (15). All enzymes that regulate ISGylation are induced by type I IFN (9). It was shown that ISGylation can occur cotranslationally on newly synthesized proteins without apparent target specificity (16). Proteins are, in general, decorated with ISG15 monomers rather than polymeric chains, and ISG15 is not a signal for proteasomal targeting (17). Rather, by competition for ubiquitin, it can protect proteins from ubiquitination and ensuing proteasomal degradation (18). However, it was shown that ISG15 can also modify ubiquitin, thus forming ISG15–ubiquitin mixed chains (19). Various signal transduction proteins can be ISGylated, and this can affect signaling outcome, as shown in some specific cases (3). Several viruses have developed distinct strategies to counteract ISGylation (7), further indicating that ISGylation plays an important role in the arms race against viral infection.

*Division of Tumor Biology and Immunology, The Netherlands Cancer Institute, 1066 CX Amsterdam, the Netherlands; [†]Department of Immunohematology and Blood Transfusion, Leiden University Medical School, 2333 ZA Leiden, the Netherlands; [‡]Oncode Institute, Leiden University Medical School, 2333 ZA Leiden, the Netherlands; and [§]Institute of Neuropathology, Faculty of Medicine, University of Freiburg, 79106 Freiburg, Germany

¹Current address: Laboratory of Mucosal Immunology, The Rockefeller University, New York, NY.

ORCID: 0000-0002-1424-1230 (T.A.); 0000-0001-9457-6438 (E.d.V.); 0000-0003-1587-1944 (K.-P.K.); 0000-0002-0569-8466 (A.V.).

Received for publication December 10, 2019. Accepted for publication February 1, 2020.

This work was supported by The Netherlands Organisation for Health Research and Development Gravitation Subgrant 00002 from the Institute for Chemical Immunology.

V.I.-G. designed the study, designed and performed experiments, analyzed and interpreted data, and wrote the manuscript; T.A. designed and performed experiments; E.d.V. designed and performed experiments; A.V. analyzed data and contributed to the manuscript; K.-P.K. contributed to the manuscript; J.B. designed the study, interpreted data, and wrote the manuscript.

Data have been deposited in the Gene Expression Omnibus (<https://www.ncbi.nlm.nih.gov/geo/>) under accession number GSE139469.

Address correspondence and reprint requests to Prof. Jannie Borst, Department of Immunohematology and Blood Transfusion, Leiden University Medical School, Albinusdreef 2, 2333 ZA Leiden, the Netherlands. E-mail address: j.g.borst@lumc.nl

The online version of this article contains supplemental material.

Abbreviations used in this article: BM, bone marrow; DC, dendritic cell; dLN, draining lymph node; GZB, granzyme B; HPV, human papilloma virus; IPA, Ingenuity Pathway Analysis; ISG, IFN-stimulated gene; MPEC, memory precursor effector cell; pDNA, plasmid DNA; SLEC, short-lived effector cell; WT, wild-type.

This article is distributed under The American Association of Immunologists, Inc., [Reuse Terms and Conditions for Author Choice articles](#).

Copyright © 2020 by The American Association of Immunologists, Inc. 0022-1767/20/\$37.50

Susceptibility to different viral infections has been studied in *Isg15*^{-/-} mice, *Ube1l*^{-/-} mice, and *Usp18*^{-/-} mice (8). Response to a number of virus types, but not all, was found to be impaired in *Isg15*^{-/-} mice. By comparing phenotypes of *Isg15*^{-/-} mice with those of *Ube1l*^{-/-} mice, in which only the conjugation to substrates, but not the function of free ISG15, is eliminated, the function of free ISG15 can be separated from that of ISGylation-dependent mechanisms. Irrespective of its protease function toward ISG15-modified substrates, USP18 represents a major negative regulator of the type I IFN response (20). Therefore, mice lacking USP18 protein expression exhibit phenotypical alterations not directly linked to ISG15. A knock-in mouse model with selective inactivation of only the protease function of USP18 exhibited enhanced ISGylation and increased viral resistance (21). From the collected work, it can be concluded that both ISGylation (22) and free ISG15 (23) can protect against certain viral infections in mice.

In the few ISG15-deficient human patients that have been reported, no evidence for increased susceptibility to viral infection has been detected so far (8). Initially, ISG15-deficient patients were discovered on basis of failed immunity to live attenuated mycobacteria (bacillus Calmette-Guérin) (5). A second group of ISG15-deficient patients that had not been vaccinated with bacillus Calmette-Guérin presented with a syndrome characterized by excessive type I IFN signaling (18), as did USP18-deficient patients (24). Mechanistic studies revealed that USP18 negatively regulates type I IFNR (IFNAR) signaling, independent of its de-ISGylation activity (18, 25). USP18 is subject to ubiquitin-dependent proteasomal degradation, which is inhibited by free intracellular ISG15. In this way, USP18 and ISG15 mediate negative feedback on IFNAR signaling, which explains the inflammatory phenotype in the ISG15-deficient patients (20). Remarkably, this stabilizing effect of free ISG15 on USP18 is found in humans, but not in mice (26), in which the affinity of the interaction is lower, likely because of the significant divergence in amino acid sequence of ISG15 between species (7).

The function of the free extracellular form of ISG15 has been an enigma. Free ISG15 does not have an N-terminal hydrophobic signal sequence (27, 28), so it is not secreted from cells in the classical way. However, ISG15 can be released from different cell types, including myeloid and lymphoid cells (5, 27–30) and is found in the serum of patients treated with type I IFN (27, 28, 31). The suggested immunomodulatory role of extracellular ISG15 is ill-defined and primarily based on cell culture experiments. ISG15 was shown to enhance IFN- γ secretion by NK cells and T cells (5, 31–33), which has been suggested to be its main antimycobacterial activity (5). A breakthrough has been the recent identification of the integrin LFA-1 (α L β 2) as cell surface receptor for extracellular ISG15. This work, performed on human cells in vitro, defined a signaling role for extracellular ISG15 by showing that 2 aa in ISG15 are critical for binding to LFA-1 and supporting IFN- γ secretion from IL-12-primed NK cells (33). One in vivo study indicates that ISG15 encoded by a DNA vaccine can promote the CTL response in mice (34), and another study reported that recombinant ISG15 protein can promote dendritic cell (DC) activation in mice (35).

We have addressed the potential role of extracellular ISG15 in supporting the CTL response in vivo and evaluated the underlying mechanisms in a clinically relevant mouse model of therapeutic vaccination. With this study, we demonstrate that extracellular ISG15 is an alarmin that promotes the CTL response via NK cells.

Materials and Methods

Mice

C57BL/6JRj mice were obtained from Janvier Laboratories (Le Genest-Saint-Isle, France). *Isg15*^{-/-} mice (36) were provided by Dr. K.-P. Knobeloch (Freiburg, Germany). In all experiments, gender- and age-matched (8–12 wk) mice were used and maintained in individually ventilated cages (Innovive, San Diego, CA). Control and test mice were selected at random. Experiments were performed according to national and institutional guidelines and approved by the institutional committee for animal experimentation.

Cells

Bone marrow (BM) cells were isolated by flushing femurs of *Isg15*^{-/-} mice with PBS supplemented with 2% FCS (Life Technologies BRL, Thermo Fisher Scientific). RBCs were lysed in 0.14 M NH₄Cl and 0.017 M Tris-HCl (pH 7.2) for 1 min. DCs were generated by culturing 2×10^6 BM cells in IMDM supplemented with 8% FCS and rFlt3 ligand (homemade) for 8 d. HeLa cells were cultured in DMEM supplemented with 8% FCS. Phoenix-Eco packaging cells were cultured in IMDM supplemented with 5% FCS.

DNA constructs and gene expression

The E7SH DNA vaccine was generated as described (37, 38). Briefly, gene fragments of the human papilloma virus (HPV)-16 E7 gene were introduced into pVAX1 vector. The cDNA-encoding mouse ISG15 wild-type (WT) (NM_015783) or ISG15 Δ GG, synthesized as a gBlock gene fragment (Integrated DNA Technologies) was inserted into the pVAX1 plasmid (Invitrogen) using BamHI and NotI restriction sites. The mutant version of ISG15, which contains a leucine instead of a tyrosine residue at position 94 and an aspartate instead of a glutamine residue at position 100 (pVAX-ISG15-Y94L_Q100D), was generated using the QuikChange kit (StrataGene) in accordance with the manufacturer's instructions. To express ISG15 variants in BM-derived DCs, ISG15 WT and Δ GG were subcloned into the pMX-IRES-GFP vector using BamHI and NotI restriction sites. BM-derived DCs expressing murine ISG15 WT or Δ GG were generated by retroviral transfection. For virus production, retroviral constructs were transfected using FuGENE HD Transfection Reagent (Promega) into Phoenix-Eco packaging cells, together with the pCL-Eco vector encoding the ecotropic retrovirus receptor. Medium that contained retrovirus was harvested from the Phoenix-Eco packaging cells 48 h later. For retroviral transduction, BM-derived DC precursors were cultured with Flt3 ligand for 3 d. Next, they were resuspended at 2×10^6 cells/ml retrovirus-containing medium plus Flt3 ligand and placed in nontissue culture-treated, 24-well plates (BD Biosciences) coated with 50 μ g/ml RetroNectin (Takara Bio). Plates were spun for 90 min at 450 \times g. Cells were cultured in this medium for 24 h. Cells were then transferred to BM-derived DC culture medium and maintained for 4 extra d before use. Transfections of cDNA in HeLa cells were performed using FuGENE HD transfection reagent (Promega) according to the manufacturer's instructions.

Western blotting

Cells were harvested, washed with PBS, and lysed in 50 mM Tris-HCl (pH 7.4), 150 mM NaCl, 1% Nonidet P-40, and cOmplete Inhibitor Cocktail (Roche). Insoluble material was removed by centrifugation at 20,000 \times g for 15 min. Protein concentration was determined by Bradford protein assay (Bio-Rad Laboratories). Equal amounts of lysate were separated on NuPAGE 4–12% Bis-Tris gels (Invitrogen), and proteins were transferred to nitrocellulose transfer packs (Bio-Rad Laboratories) using the Semi-dry Trans-Blot Turbo Transfer System (Bio-Rad Laboratories) according to manufacturer's instructions. Membranes were blocked with Roche Western block solution (1:10) in TBS with 0.1% Tween 20 for 1 h at room temperature. Next, membranes were incubated overnight at 4°C with appropriate primary Abs in Roche Western block solution (1:20)/TBS with 0.1% Tween 20, washed with TBS with 0.1% Tween 20, and probed with the adequate secondary Abs (1:10,000) in Roche Western block solution/TBS with 0.1% Tween 20 for 1 h at room temperature. Primary Abs used were the following: rabbit anti-mouse ISG15 (1:5000, kindly provided by Dr. K.-P. Knobeloch), mouse anti-actin (1:10,000, clone C4; MAB1501R; MilliporeSigma), and anti-mouse GAPDH (1:2000, clone D4C6R; 97166S; Cell Signaling Technology). Secondary Abs used were the following: goat anti-mouse IRDye 682/800 (925-68070/926-32210) or goat anti-rabbit IRDye 682/800 (925-68071/925-32211) from LI-COR Biosciences.

Immunoblots were developed with the aid of an Odyssey Imaging System (LI-COR Biosciences).

Intraepidermal DNA “tattoo” vaccination

On day 0, mice were anesthetized with isoflurane, and the hair on a hind leg was removed using depilating cream (Vee; Reckitt Benckiser). On days 0, 3, and 6, a 15- μ l drop of a solution containing 2 mg/ml plasmid DNA (pDNA) mixture in 10 mM Tris-HCl and 1 mM EDTA (pH 8) was applied to the hairless skin of anesthetized animals and delivered into the epidermis with a Permanent Makeup Tattoo machine (MT.DERM) using a sterile disposable nine-needle bar with a needle depth of 1 mm and an oscillating frequency of 100 Hz for 45 s.

In vivo NK cell depletion

Mice were injected i.v. with 100 μ l of anti-asialo GM1 (39) or control rabbit sera (Wako Chemicals) diluted 1:10 in HBSS the day before the first DNA vaccination and on days 0 and 3.

Leukocyte isolation and flow cytometry

Blood was collected from tail bleeding using Microvette CB 300 LH tubes (Sarstedt). To isolate lymphocytes from spleen and inguinal draining lymph node (dLN), organs were passed through a 70- μ m cell strainer (BD Falcon). RBCs were lysed in 0.14 M NH_4Cl and 0.017 M Tris-HCl (pH 7.2) for 1 min at room temperature. Then, cell samples were centrifuged for 5 min at $400 \times g$ and resuspended in FACS buffer (PBS with 2% FCS; Antibody Production Services). Surface staining with relevant mAbs and allophycocyanin-H-2D^b/E7₄₉₋₅₇ tetramers was performed for 30 min on ice. Intracellular staining was performed after cell fixation and permeabilization using Foxp3 Transcription Factor Staining Buffer Set (eBioscience). Fluorochrome-labeled mAbs employed were as follows: anti-CD8 α -V500 (1:200, clone 53-6.7) and anti-IFN- γ -eF450 (1:100, clone XMG1.2) from BD Biosciences; anti-CD127-BV421 (1:200, clone A7R34) and anti-CD3-Alexa Fluor 488 (1:200, clone 17A2) from BioLegend; anti-KLRG1-PEeF610 (1:200, clone 2F1), anti-CD44-PerCP-Cy5.5 (1:400, clone IM7), anti-CD49b-PE-Cy7 (1:200, clone DX5), anti-NK1.1-Alexa Fluor 700 (1:200, clone PK136), anti-CD4-eF450 (1:200, clone GK1.5), anti-Tbet-PE-Cy7, and anti-CD62L-FITC (1:100, MEL-14), from eBioscience; and anti-granzyme B (GZB)-PE (1:200, clone CLB-GB11) (Sanquin Reagents). To detect cytokine production by E7₄₉₋₅₇-specific CD8⁺ T cells in dLN and spleen, cells were incubated for 16 h with 1 μ g/ml E7₄₉₋₅₇ or no peptide (negative control) in the presence of GolgiPlug (BD Biosciences) in IMDM supplemented with 8% FCS. Flow cytometry was performed using LSRFortessa (BD Biosciences), and data were analyzed with FlowJo software (Tree Star). Live cells were selected based on staining with LIVE/DEAD Near Infrared dye (Thermo Fisher Scientific).

RNA preparation and sequencing

At day 4 postvaccination, total skin from the tattooed area was isolated, and total RNA was isolated using the RNeasy Mini Kit (catalog no. 74106; QIAGEN), including an on-column DNA digestion (catalog no. 79254; QIAGEN), according to the manufacturer's instructions. Quality and quantity of the total RNA was assessed by the 2100 Bioanalyzer using an RNA Nano Chip and RNA Pico Chip (Agilent Technologies). Total RNA samples having RNA integrity number > 8 were subjected to library generation. Strand-specific cDNA libraries were generated using the TruSeq Stranded mRNA Sample Preparation Kit (Illumina) according to the manufacturer's instructions. The libraries were analyzed on a 2100 Bioanalyzer using a DNA 7500 Chip (Agilent Technologies), diluted and pooled equimolar into a multiplex sequencing pool and stored at -20°C . The libraries were sequenced with 65 base single reads on a HiSeq 2500 using V4 chemistry (Illumina).

RNA sequence analysis

Differential expression of genes was assessed using the DESeq2 package (40) using default parameters in R v.3.5.3 (<https://www.R-project.org/>). Genes with adjusted p values ≤ 0.05 were deemed significantly differentially expressed. To find activated pathways, overexpressed in comparison with the control (according to log-fold change > 0 , adjusted p value ≤ 0.1), were used as input for enrichment analysis using the Reactome enrichment analysis tool available at <https://reactome.org/PathwayBrowser/#TOOL=AT>. Additionally, we analyzed activated pathways using Ingenuity Pathway Analysis (IPA; QIAGEN). In this case, raw read counts were loaded into the software and analysis carried out using default settings. Data have been deposited in the Gene Expression

Omnibus database (<https://www.ncbi.nlm.nih.gov/geo/>) under accession number GSE139469.

Statistical analysis

Statistical significance was determined with GraphPad Prism software as indicated in the figure legends.

Illustrations

Illustrations in Figs. 1A, 2A, and 6A were made with BioRender.

Results

ISG15 causes innate immune alert in the skin

We were intrigued by earlier findings that extracellular ISG15 may act as an adjuvant to support the CTL response (34). We aimed to corroborate this and to understand the mechanistic basis, making use of a versatile therapeutic DNA vaccination model in mice (37) that we have well characterized previously (38, 41, 42). In this model, pDNA is applied on the depilated skin and injected into the epidermis using a tattoo device (Fig. 1A). This results in transfection of keratinocytes with the pDNA of interest, which is subsequently transcribed and translated (42). To determine whether ISG15 protein expression had a local effect on the vaccinated skin, we performed the following experiment: two groups of mice were vaccinated with pDNA encoding specific Ag (to be described in Fig. 2) combined with pDNA encoding ISG15 or an equal dose of empty vector (Fig. 1A). At day 4 after vaccination, total skin from the area of vaccination was excised, and mRNA was isolated and subjected to deep sequencing.

Statistical analysis of normalized transcript read counts showed that 444 genes were differentially expressed in the skin as a result of ISG15 coexpression (Supplemental Table I; Gene Expression Omnibus submission GSE139469). Using IPA, we identified 29 functional categories predicted to be increased according to an activation z -score ≥ 2 . Interestingly, 15 of these categories indicated that ISG15 stimulated cell migration, particularly of myeloid cells and endothelial cells (Fig. 1B). A zoom-in on the 140 specific molecules in the functional categories listed in Fig. 1B highlighted that ISG15 significantly upregulated the expression of various metalloproteases (Mmp2, Mmp9, Mmp11, Mmp14, and Adam12; downregulation of inhibitor Timp4) and collagens (Colla1, Col3a1, Col6a1, and Coll8a1) (Fig. 1C), suggesting remodeling of the extracellular matrix. This correlated with gene ontology analysis using Reactome, which more precisely specified metalloprotease activity, collagen degradation and formation, and extracellular matrix organization (Table I). The extracellular matrix remodeling and immune cell signature observed in the transcriptome strongly suggests that ISG15 is able to evoke tissue alarm.

WT ISG15 promotes the CD8⁺ T cell response to therapeutic vaccination

Using a fluorescent protein encoded by the vaccine, we have previously shown that vaccine protein expressed by keratinocytes can reach the proximal skin-draining dLN in two ways: the protein can be transported by migratory dermal DCs or drain passively via the lymph (42). In both cases, DCs can process the vaccine protein and cross-present relevant peptides in MHC class I, which can lead to the activation of Ag-specific CD8⁺ T cells (Fig. 2A). To examine CD8⁺ T cell activation, we used a DNA vaccine-encoding HPV-16 E7 protein in a shuffled configuration (E7SH) (37, 38). This protein contains an immunodominant epitope, E7₄₉₋₅₇, that is presented by H-2D^b (Fig. 2B).

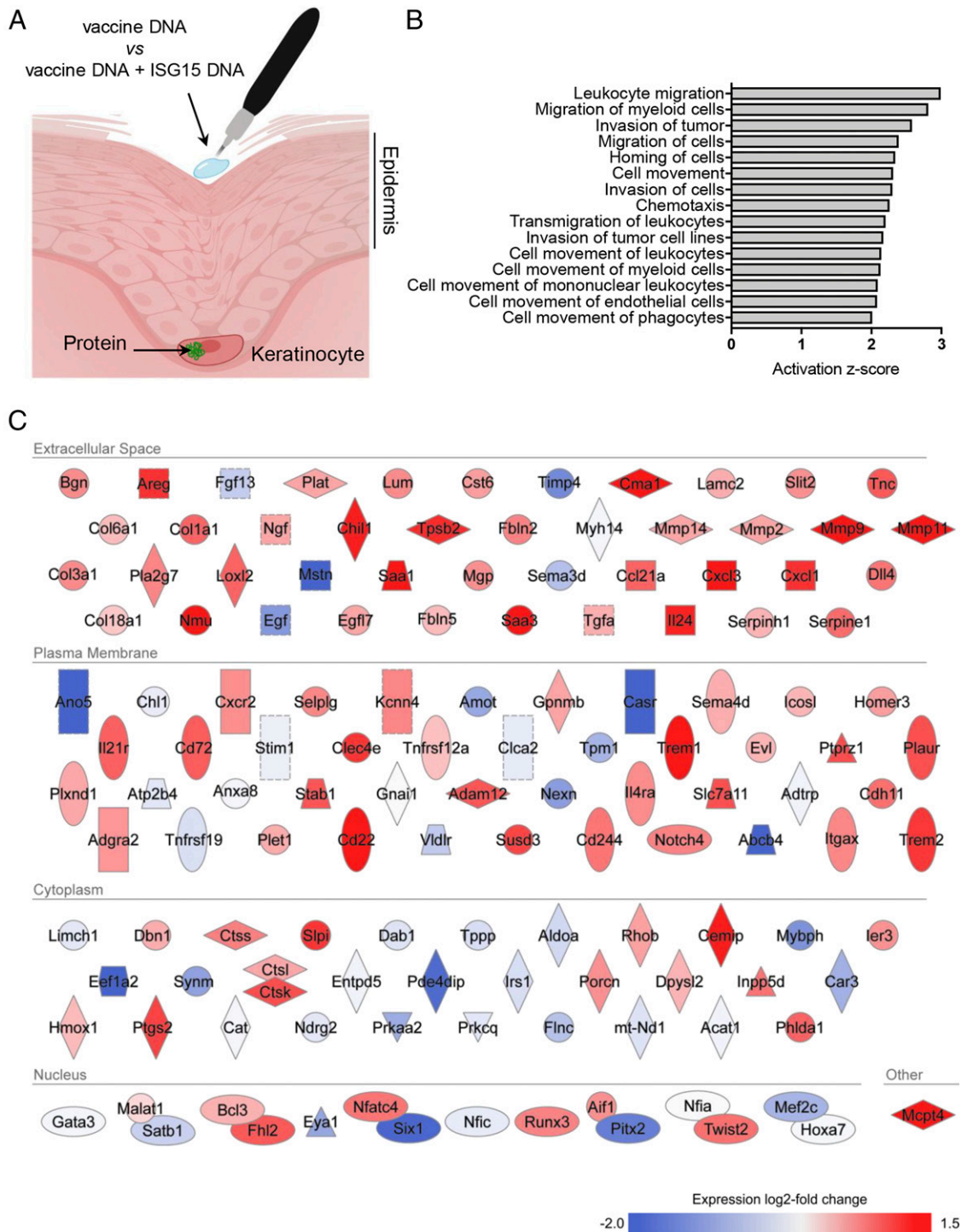


FIGURE 1. The skin transcriptome reports ISG15 activity. **(A)** Illustration of the intraepidermal pDNA tattoo vaccination procedure and expression of pDNA-encoded protein (green) in transfected keratinocytes. Mice were vaccinated in comparative settings with pDNA encoding HPV-E7 (vaccine DNA) in combination with either pDNA-encoding ISG15 ΔGG (ISG15 DNA) or an equal amount of empty vector pDNA. **(B)** mRNA from total skin of mice ($n = 3$ per group) vaccinated with “vaccine DNA” versus “vaccine DNA + ISG15 DNA” was subjected to deep sequencing. Gene ontology analysis was performed by IPA of the 444 genes found to be differentially expressed between the comparative vaccination settings (p value ≤ 0.05). The functional categories connected to cell migration and with a predictive activation z -score ≥ 2 are depicted. **(C)** IPA-based rendering of differentially expressed molecules from the functional categories depicted in **(B)** and their subcellular localization. The total experiment was performed once.

To examine the effect of ISG15 on the T cell response, we vaccinated the mice with the E7SH vaccine in combination with empty vector or vector encoding WT ISG15. We followed the CD8⁺ T cell response by flow cytometry, using MHC tetramers (Fig. 2C). We knew that vaccination with E7SH elicits a weak CTL response (38, 41) and purposely used this vaccination

setting to create a good window for testing the potential adjuvant effect of ISG15. The E7-specific CD8⁺ T cell response was followed in blood over time (Fig. 2D). This analysis revealed that the frequency of E7-specific cells within total CD8⁺ T cells was dramatically increased in the ISG15-adjuvanted setting. Analysis for expression of the CTL effector molecule GZB at

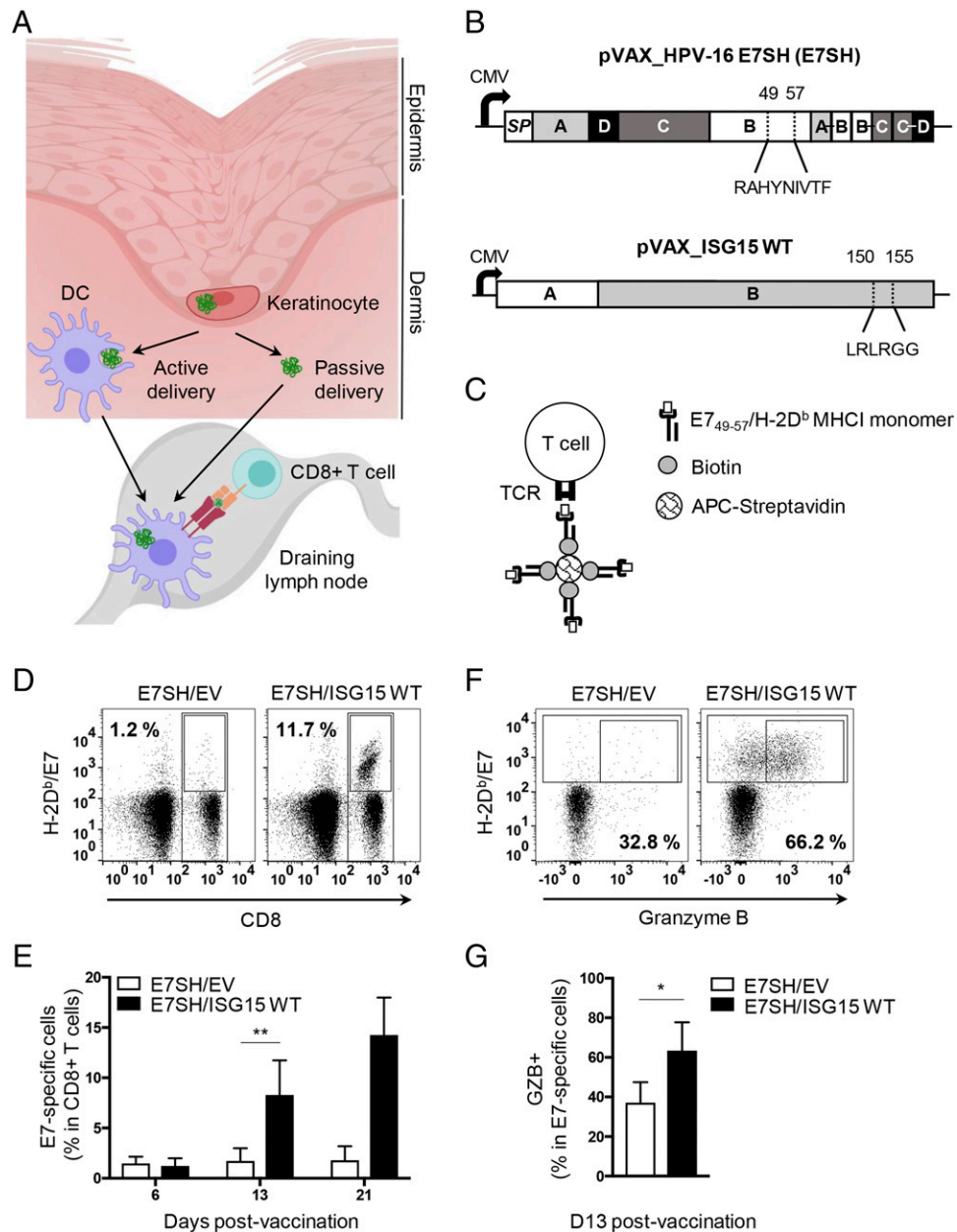


FIGURE 2. WT ISG15 promotes the Ag-specific CTL response to vaccination. **(A)** Illustration of the cellular context of vaccine Ag delivery in the skin and the route of the Ag from keratinocytes to the dLN. **(B)** Scheme of the DNA sequence encoding the shuffled (SH) version of the HPV-16 E7 protein (E7SH vaccine) and ISG15 WT used for vaccination. For the E7 protein, the different exons (A–D) and the signal peptide (SP) are indicated. In exon B, the immunodominant H-2D^b-restricted epitope RAHYNIVTF (corresponding to aa 49–57 from the original E7 protein) is depicted (37, 38). For ISG15, the two exons (A and B) are indicated (ENSMUST00000085425.5). In exon B, the conjugation site (LRLRGG, aa 150–155) is depicted. **(C)** MHC tetramer technology to identify by flow cytometry CD8⁺ T cells with a TCR that recognizes H-2D^b/E7_{49–57}. Recombinant H-2D^b MHC class I (MHCI) monomers are folded with E7_{49–57} peptide, conjugated to biotin and multimerized with streptavidin conjugated to a fluorophore allophycocyanin. **(D–G)** Mice ($n = 5$ per group) were vaccinated with HPV-16 E7SH cDNA (E7SH) in combination with pVAX empty vector (EV) or pVAX-mouse ISG15 (ISG15 WT) on days 0, 3, and 6. The CD8⁺ T cell response was followed in time by flow cytometric analysis of peripheral blood using H-2D^b/E7_{49–57} tetramers. **(D)** Representative staining of cells with H-2D^b/E7_{49–57} tetramer and anti-CD8 Ab. Numbers indicate frequency of tetramer⁺ cells among total CD8⁺ T cells. **(E)** Quantification of the percentage of H-2D^b/E7_{49–57} tetramer⁺ cells among total CD8⁺ T cells over time postvaccination. **(F)** Representative staining of cells with H-2D^b/E7_{49–57} tetramer and Ab to GZB. Numbers indicate percentage of GZB⁺ cells among tetramer⁺ cells. **(G)** Quantification of the percentage of GZB⁺ cells among tetramer⁺ cells at day 13 postvaccination. Results are representative of at least three experiments. Statistical analysis was performed using two-tailed Student *t* test. * $p < 0.05$, ** $p < 0.01$.

day 13 emphasized that more CTLs were raised in the ISG15-adjuvanted setting (Fig. 2E).

Free ISG15 enhances the generation of vaccine Ag-specific CTLs

We next examined whether it was free or conjugated ISG15 that promoted the CTL response. For this purpose, we compared the

activity of ISG15 WT with the activity of the ISG15 Δ GG mutant that lacks the C-terminal glycine residues that are required for substrate conjugation (Fig. 3A). Lack of ISG15 conjugation was validated by expression of ISG15 WT and the ISG15 Δ GG mutant in *Isig15*^{-/-} DCs. As expected, transduction of a vector encoding ISG15 WT led to expression of the free form as well as ISG15 conjugation to multiple proteins, whereas transduction of

Table I. Gene ontology analysis of ISG15-induced differential gene expression in skin

Pathway Name	No. Entities Found	No. Entities Total	<i>p</i> Value	False Discovery Rate
Collagen degradation	15	57	6.35×10^{-13}	1.13×10^{-10}
Extracellular matrix organization	29	295	6.87×10^{-13}	1.13×10^{-10}
Assembly of collagen fibrils and other multimeric structures	14	61	2.28×10^{-11}	2.49×10^{-9}
Degradation of extracellular matrix	18	135	1.97×10^{-10}	1.62×10^{-8}
Collagen formation	15	88	2.57×10^{-10}	1.67×10^{-8}
Collagen biosynthesis and modifying enzymes	11	64	6.17×10^{-8}	3.33×10^{-6}
Extracellular matrix proteoglycans	10	51	7.50×10^{-8}	3.53×10^{-6}
Collagen chain trimerization	9	41	1.34×10^{-13}	5.48×10^{-6}
Integrin cell surface interactions	11	81	6.22×10^{-7}	2.24×10^{-5}
NCAM1 interactions	6	22	5.13×10^{-6}	1.64×10^{-4}
Activation of matrix metalloproteases	7	51	6.72×10^{-5}	0.00195
Axon guidance	16	272	8.23×10^{-5}	0.00222
Signaling by PDGF	7	57	1.33×10^{-4}	0.00321
NCAM signaling for neurite outgrowth	6	40	1.39×10^{-4}	0.00321
Other semaphorin interactions	4	14	1.71×10^{-4}	0.00359

Pathway analysis using Reactome overrepresentation analysis of the 254 overexpressed genes (log fold change > 0 out of the total of 444 differentially expressed genes in Fig. 1B). The top 15 pathways are depicted.

the vector encoding ISG15 Δ GG led to expression of the free form only (Fig. 3B).

The CD8⁺ T cell response to vaccination with E7SH was increased in equal measure by concomitant vaccination with either ISG15 WT or ISG15 Δ GG throughout the entire kinetics, as monitored in blood (Fig. 3C). The CD8⁺ T cells raised after ISG15-adjuvanted vaccination had undergone CTL effector differentiation, as determined by expression of GZB and the transcription factor Tbet and the effector phenotype CD44⁺CD62L⁻ (Fig. 3D). Both ISG15 WT and nonconjugatable ISG15 Δ GG promoted the CTL response in equal measure (Fig. 3C, 3D).

To validate that the increased magnitude of the CTL response observed in blood was a consequence of an increase in CD8⁺ T cell priming, we examined the response in dLN and spleen. Both ISG15 WT and ISG15 Δ GG significantly increased, in equal measure, the magnitude of the E7-specific CD8⁺ T cell response in dLN and spleen (Fig. 3E). Furthermore, the responder CD8⁺ T cells had differentiated into CTLs as determined on day 16 by expression of GZB and coexpression of IFN- γ and TNF- α (Fig. 3E). This analysis highlighted that vaccination with E7SH alone hardly generated functional CTLs, whereas ISG15 WT or ISG15 Δ GG-adjuvanted vaccination raised a sizeable CTL response. We conclude that ISG15 does not need to be conjugated to proteins to have an adjuvant effect on the CTL response to vaccination.

Free ISG15 enhances CTL differentiation, formation of short-lived effector and effector memory CTLs

To examine the impact of ISG15 on the intrinsic functionality of CTLs, we analyzed the protein expression levels of GZB, Tbet, and CD44 on a per-cell basis. In the ISG15-adjuvanted settings (WT or Δ GG), CTLs expressed higher levels of these molecules, indicating improved effector differentiation (Fig. 4A). Furthermore, we determined the formation of short-lived effector cells (SLECs) and memory precursor effector cells (MPECs) throughout the primary immune response. ISG15 WT and Δ GG increased in equal measure the frequency of SLECs (KLRG1⁺ CD127) within E7-specific CD8⁺ T cell pool raised upon vaccination, as measured in blood throughout the entire response kinetics. The frequency of MPECs (CD127⁺KLRG1⁻) within the E7-specific CD8⁺ T cell pool was correspondingly reduced in both ISG15-adjuvanted settings (Fig. 4B, 4C). Thus, CTL differentiation seemed to be geared more toward a short-lived effector- than an effector memory differentiation fate in the ISG15-adjuvanted setting. Nevertheless, the absolute numbers of E7-specific MPECs in

spleen at day 16 postvaccination were significantly higher when ISG15 was included in the vaccination setting (Fig. 4D). This result correlated with an increased frequency of E7-specific CD8⁺ T cells in blood at day 72 postvaccination (steady-state memory) (Fig. 4E). Among these memory cells, effector memory phenotype cells (CD44⁺CD62L⁻) were drastically increased in the ISG15-adjuvanted setting (Fig. 4F). Thus, free ISG15 promotes the effector differentiation of CTLs, the formation of short-lived effector CTLs, as well as the formation of memory precursor effector CTLs and effector memory CTLs.

Amino acid residues Y94 and Q100 of ISG15 are required for its adjuvant effect on the CTL response

Recently, the integrin LFA-1 has been defined as a receptor for free ISG15 in a human cell culture system. Amino acid residues Y96 and Q102 in human ISG15 proved to be critical for LFA-1 binding (33) (Fig. 5A). Based on these findings, we hypothesized that the effect of free ISG15 on the CTL response that we observed in this study *in vivo* is a consequence of ISG15 binding to a receptor. We therefore tested the adjuvant activity of mouse ISG15 with the equivalent mutations, Y94L_Q100D (Fig. 5A), that should abrogate its ligand activity. The mutant, encoded by the pVAX expression vector, was expressed to at least equivalent levels as WT ISG15 at the protein level in transfected cells (Fig. 5B).

Mice were vaccinated as described above with a vector encoding E7SH, in conjunction with either empty vector, vector encoding ISG15 WT, or ISG15 Y94L_Q100D. The E7-specific CD8⁺ T cell response was followed in blood over time. The two mutations in ISG15 completely abrogated its ability to improve the E7-specific CD8⁺ T cell response, as determined by response magnitude (Fig. 5C), generation of E7-specific GZB⁺ cells (Fig. 5D), and intrinsic CTL quality, as defined by GZB expression on a per cell basis (Fig. 5E).

ISG15 promotes the CTL response via NK cells

In the same study based on human cells culture as referred above (33), extracellular recombinant ISG15 was shown to promote IFN- γ production from IL-12-primed NK cells by binding to LFA-1 (Fig. 6A). We therefore examined whether ISG15 acted via NK cells to improve the CTL response in our vaccination setting. For this purpose, NK cells were depleted with antiserum to glycolipid asialo GM1 (39) before and during the vaccination regimen. This depletion did not affect CD8⁺ T cells (Fig. 6B) and was very effective in NK cell depletion as measured in blood throughout the T cell response kinetics (Fig. 6C). Interestingly, the response to

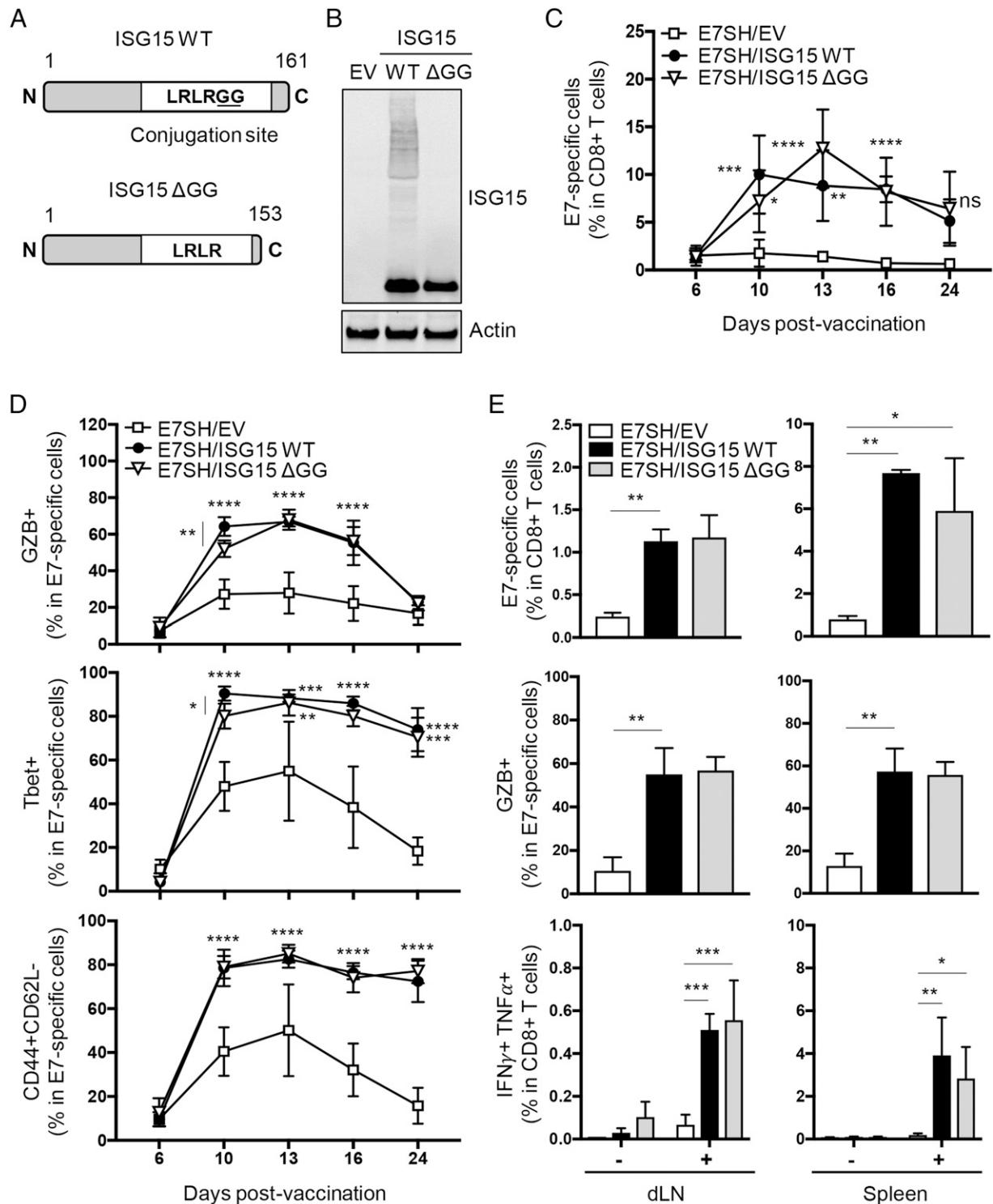


FIGURE 3. The free form of ISG15 promotes CTL priming in response to vaccination. **(A)** Scheme of mouse ISG15 WT protein (aa 1–161) and its C-terminal truncated version, ISG15 Δ GG (aa 1–153). The minimal sequence (LRLRGG) required for its conjugation to intracellular proteins is depicted in ISG15 WT. **(B)** Validation of ISG15 constructs by assessment of ISGylation of intracellular proteins. pDNA encoding ISG15 WT or ISG15 Δ GG and empty control vector (EV) were expressed in *Isig15*^{-/-} BM-derived DCs, and ISGylation was assessed by Western blotting on total cell lysates. Actin served as loading control. Results are representative of multiple independent analyses with individual samples. **(C–E)** Mice ($n = 7$ per group) were vaccinated with plasmid encoding E7SH, either combined with EV, ISG15 WT, or ISG15 Δ GG as outlined in Fig. 2. **(C and D)** The E7-specific CTL response was followed over time in peripheral blood by flow cytometric analysis using H-2D^b/E7_{49–57} tetramers and Abs to CD8, GZB, Tbet, CD44, and CD62L. **(C)** Quantification of the percentage of H-2D^b/E7_{49–57} tetramer⁺ cells among total CD8⁺ T cells. **(D)** Quantification of the percentage of GZB⁺, Tbet⁺, and CD44⁺CD62L⁻ cells within H-2D^b/E7_{49–57} tetramer⁺ cells. **(E)** On day 16, three mice per group were sacrificed, and the T cell response was assessed in dLN and spleen. Depicted are percentage of H-2D^b/E7_{49–57} tetramer⁺ cells within total CD8⁺ T cells, percentage of GZB⁺ cells within tetramer⁺ cells ex vivo, and percentage of IFN- γ ⁺TNF- α ⁺ cells among total CD8⁺T cells after in vitro stimulation. Results are representative of two experiments. Statistical analysis was performed using one-way ANOVA (C and D) or two-way ANOVA (E) and Tukey posttest. * $p < 0.05$, ** $p < 0.01$, *** $p < 0.001$, **** $p < 0.0001$.

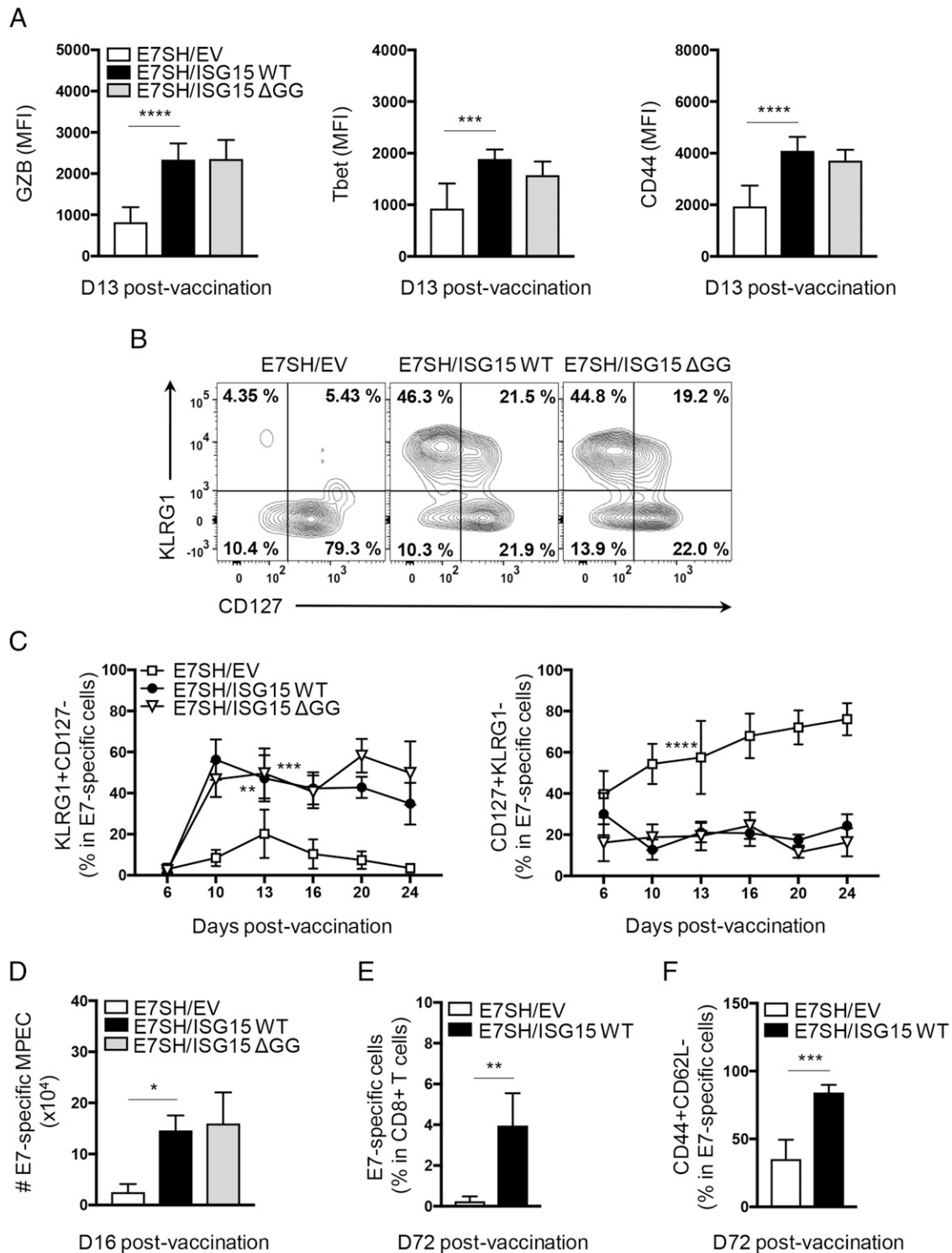


FIGURE 4. The free form of ISG15 supports short-lived effector and effector memory differentiation of CTLs. **(A–D)** Mice ($n = 7$ per group) were vaccinated with plasmid encoding E7SH, either combined with EV, ISG15 WT, or ISG15 Δ GG as outlined in Fig. 2. **(A)** Flow cytometric analysis of protein expression as assessed by mean fluorescence intensity (MFI) of GZB, Tbet, and CD44 on E7-specific CD8⁺ T cells in blood at day 13 postvaccination. **(B)** Representative flow cytometric analysis of E7-specific CD8⁺ T cells stained with Abs to KLRG1 and CD127. Numbers indicate percentage of cells in each quadrant. **(C)** Quantification of percentage of SLECs (KLRG1⁺CD127⁻) (left) and MPECs (CD127⁺KLRG1⁻) (right) within E7-specific CD8⁺ T cells in blood over time. **(D)** On day 16, three mice per group were sacrificed, and total numbers of CD127⁺KLRG1⁻ E7-specific cells per spleen were determined. **(E)** Quantification of the percentage of E7-specific cells within CD8⁺ T cells in blood on day 72. **(F)** Quantification of the percentage of CD44⁺CD62L⁻ cells among E7-specific CD8⁺ T cells in blood on day 72. Results are representative of two experiments. Statistical analysis was performed using one-way ANOVA and Tukey posttest (A–D) or two-tailed Student t test (E). * $p < 0.05$, ** $p < 0.01$, *** $p < 0.001$, **** $p < 0.0001$.

vaccination with E7SH in combination with ISG15 WT was significantly reduced upon NK cell depletion (Fig. 6D). In the NK cell-depleted setting, the E7-specific CD8⁺ T cell response was

negligible until day 10, which was the peak of the response in the control setting. At day 13 postvaccination, the CD8⁺ T cell response reached its peak in the NK cell-depleted setting, which

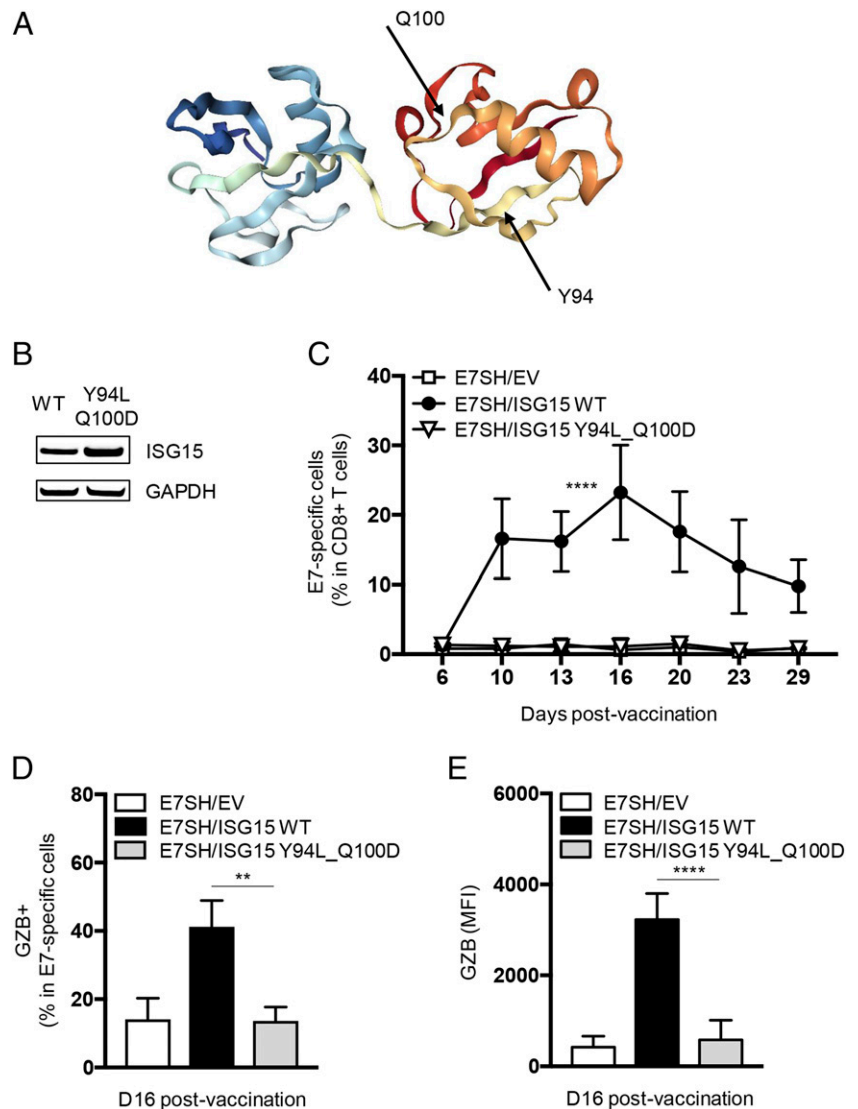


FIGURE 5. Residues Y94 and Q100 in ISG15 are critical for its adjuvant effect on the CTL response. **(A)** Three-dimensional structure of ISG15 and the position of amino acids Y94 and Q100 (<http://www.rcsb.org/structure/5TLA>) (61). **(B)** Validation of equal expression of WT and Y94L_Q100D mutant ISG15 constructs in HeLa cells, as determined by Western blotting on total cell lysates. GAPDH was used as loading control. Results are representative of two analyses with individual samples. **(C–E)** Mice ($n = 4$ per group) were vaccinated with plasmid encoding E7SH, either combined with EV, ISG15 WT, or ISG15 Y94L_Q100D as outlined in Fig. 2. **(C)** Quantification of the E7-specific CD8⁺ T cell response over time in blood. **(D)** Quantification of the percentage of GZB⁺ cells among H-2D^b/E7_{49–57} tetramer⁺ cells at day 16. **(E)** Protein quantification (mean fluorescence intensity [MFI]) of GZB in H-2D^b/E7_{49–57} tetramer⁺ cells at day 16. Results are representative of two experiments. Statistical analysis was performed using one-way ANOVA and Tukey posttest and is indicated for day 16. ** $p < 0.01$, **** $p < 0.0001$.

was lower than in the control setting. Furthermore, NK cell depletion led to a significant reduction in the frequency of SLECs and a corresponding increase in MPECs at day 10 of the response, but no differences in SLEC and MPEC frequencies were evident at day 13 in the control and NK cell-depleted settings (Fig. 6E). This indicates that the CTLs were capable of acquiring an effector phenotype in the absence of NK cells. Thus, in absence of NK cells, the effects of ISG15 on the magnitude and effector quality of the CTL response were delayed. However, the response was not fully abrogated as in case of the ISG15 Y94L_Q100D mutant, suggesting that ISG15 additionally stimulates the CD8⁺ T cell response in an NK cell-independent manner.

Discussion

In the current study, we have identified a tissue-wide response to free ISG15. Gene expression profiling demonstrated that expression of ISG15 Δ GG in the epidermis stimulated the migration of innate immune cells and endothelial cells, as well as extracellular matrix degradation and remodeling. Endogenous ISG15 has been implicated in migration of different cancer cell lines (43). Furthermore, recombinant ISG15 was found to induce neutrophil chemotaxis in vitro (44) and influx of DCs to the site of infection in vivo (34). The gene expression signature induced by free ISG15 in the skin suggested myeloid cell recruitment and

proinflammatory activity according to the upregulation of the cell surface receptors Trem1 and Trem2 (45). Free ISG15 promoted inflammation also as judged by the upregulation of chemokines CXCL1 and CXCL3, which are produced by neutrophils and promote vascular leakage (46), as well as the upregulation of IL-21R, which responds to T cell-derived IL-21 by induction of proinflammatory cytokines (47). However, the gene signature also suggested epithelial tissue repair, as indicated by collagen synthesis and increased expression of IL-24 (48) and ICOSL (49). Its collective properties as a molecule that is released from cells following pathogen challenge and/or cell death and is able to mobilize and activate various leukocytes suggest that free ISG15 acts as an alarmin (50), as has been proposed earlier (51). Another criterion to classify ISG15 as an alarmin is that the candidate molecule is able to activate innate and adaptive immune responses, which we indeed show to be the case for free ISG15. In our gene set obtained from the vaccinated skin, we did not observe upregulation of IL-10 or IL-6 that were previously shown to be produced by human blood-derived monocytes in response to extracellular ISG15 (51). We also did not find IFN- γ that can be produced by human blood-derived lymphoid cells in response to extracellular ISG15 (31–33). This may be explained by the fact that we determine a response in the skin rather than peripheral blood.

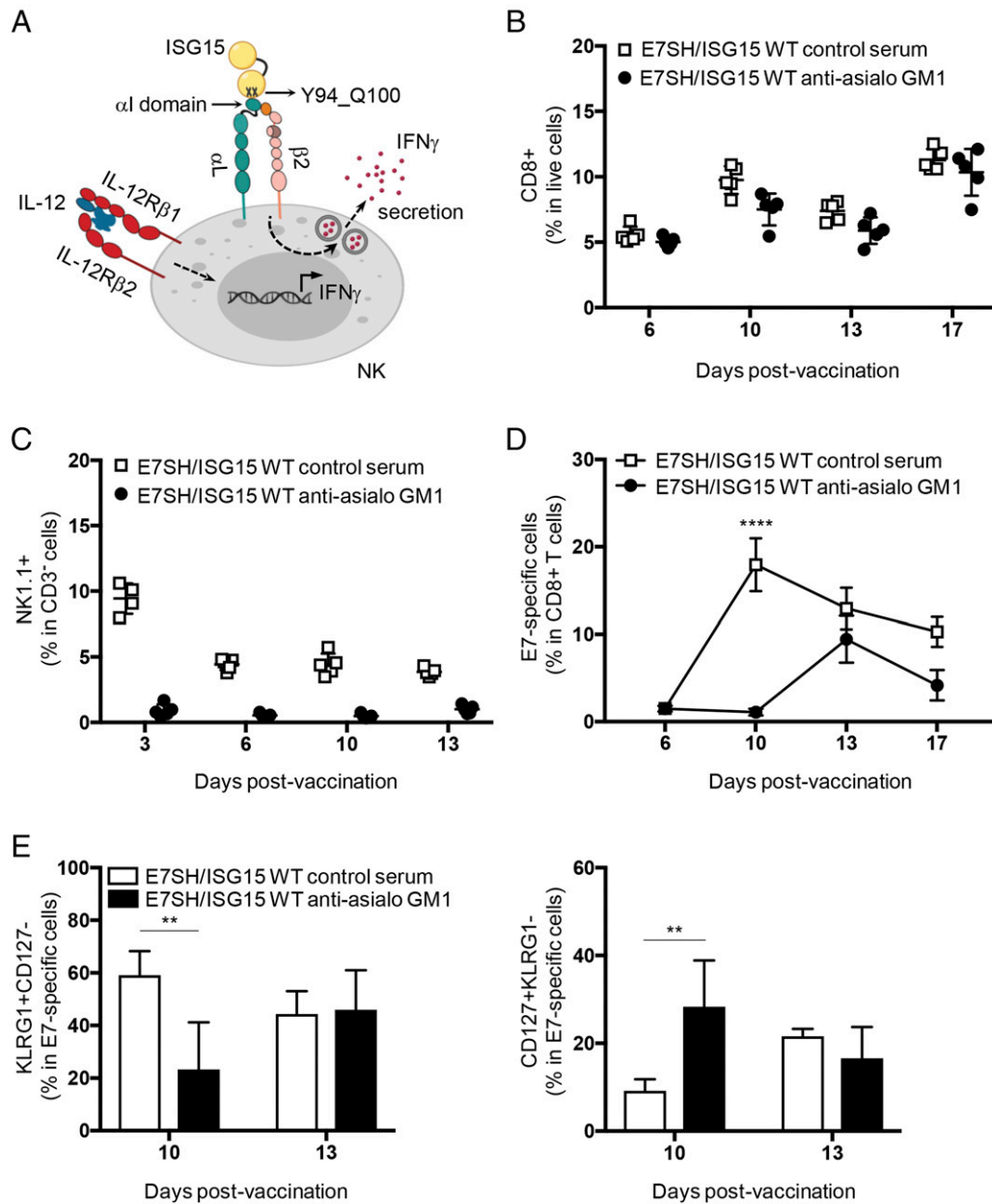


FIGURE 6. NK cells contribute to relaying the effects of ISG15 to E7-specific CD8⁺ T cells. (A) Scheme showing ISG15 interaction with LFA-1 (α L β 2 integrin and CD11a/CD18) receptor in NK cells and its biological impact as described for human cells in vitro (33). (B–E) Mice ($n = 4$ per group) were vaccinated on days 0, 3, and 6 with plasmid encoding E7SH combined with ISG15 WT. On days $-1, 0, 3,$ and $6,$ mice were injected i.v. with control serum or anti-asialo GM1 antiserum. (B) Frequency of CD8⁺ cells among live cells in blood at the indicated days postvaccination. (C) Frequency of NK1.1⁺ cells within CD3-negative cells in blood at the indicated days postvaccination to validate NK cell depletion. (D) E7-specific cells within CD8⁺ cells in blood at the indicated days postvaccination. (E) Percentage of SLECs (KLRG1⁺CD127⁻) (left) and MPECs (CD127⁺KLRG1⁻) (right) within E7-specific CD8⁺ T cells in blood at days 10 and 13. Results are representative of two experiments. Statistical evaluation was performed using one-way ANOVA evaluation and Tukey posttest and is indicated for day 10. ** $p < 0.01,$ **** $p < 0.0001.$

Vaccination using an MHC class I epitope only is known to be ineffective in eliciting a CTL response. That is why MHC class II-binding helper epitopes are included in therapeutic vaccines to cancer and infectious disease (52). An optimal CTL response to vaccination relies on cross-presentation and activation of the DCs presenting the vaccine Ag by CD4⁺ T cells (53). We and others have shown previously in the DNA vaccination model presented in this study how inclusion of helper epitopes supports the CTL response (37, 38, 41). In the current study, we find that free ISG15 can improve the CTL response to the vaccine as an alternative to CD4⁺ T cell help. Moreover, we find that this adjuvant activity depends on residues Y94 and Q100 of mouse ISG15, whose

equivalents were implicated in LFA-1 binding in a human in vitro system (33). We now show that the in vivo function of free ISG15 depends on these amino acids. The fact that free ISG15 needs these residues to bind to LFA-1 in vitro and to optimize the CTL response in vivo supports the concept that free ISG15 acts extracellularly as an immunomodulatory molecule. Remarkably, we found that free ISG15 promoted the vaccine-specific CTL response, at least in part, via NK cells. This is in further agreement with the study of Swaim et al. (33), which found free ISG15 to promote human NK cell function in vitro.

In our study, free ISG15 promoted the clonal expansion of CD8⁺ T cells that respond to the vaccine, as well as their differentiation

into SLECs and effector memory cells. The improved effector quality of CTLs primed in presence of free ISG15 was testified by the increased expression of GZB on a per-cell basis. CD4⁺ T cell help also promotes the CTL response in this manner, but the “help” delivered by ISG15 was CD4⁺ T cell independent, because we have shown that CD4⁺ T cells do not respond to the vaccine that we have employed in the current study (38). Our findings are consistent with those of other authors who found that free ISG15 promoted the CTL response in a setting with i.m. DNA vaccination (34) that is less robust than intraepidermal vaccination (54). In our study, we show the underlying mechanisms. As discussed above, free ISG15 caused a tissue alert and promoted the CTL response. Free ISG15 may have acted directly on CD8⁺ T cells to promote their response, but, more likely, given the myeloid cell activity induced, DC function was affected. The limiting factor in the CTL response in this model is the appropriate activation of DCs. Migratory cDC1 deliver the vaccine Ag from the skin to the dLNs, and a deficiency in their activation limits the CTL response to vaccination (42). We hypothesize that free ISG15 acts as an alarmin in the skin, promoting an inflammatory phenotype and creating the required signals for adequate activation of migratory cDC1s presenting the vaccine Ag.

Free ISG15 proved to act, at least in part, via NK cells to optimize the CTL response. NK cells and DCs are known to communicate in a bidirectional fashion: DCs can help activate NK cells and thereby promote innate immunity, and reciprocally, NK cells can help activate DCs and thereby promote adaptive immunity (55). Therefore, we hypothesize that ISG15 impacts NK cell–DC cross-talk and thereby creates an optimal CTL response. This cross-talk may take place in the skin, because NK cells have been found in both healthy and inflamed skin (56, 57), and migratory DCs are known to play a role in our vaccination model (42). Therefore, in our model, ISG15 may have promoted IFN- γ production by NK cells, which is known to enhance expression of costimulatory molecules and IL-12 by DCs (58). The (migratory) DCs would thereby be optimized for CTL priming. Because NK cell depletion did not fully abrogate the ISG15 effect on the CTL response in our model in contrast to mutation of Y94 and Q100, ISG15 likely acts as an immunostimulatory ligand on other cells as well. NKT cells are a good candidate, because this cell type was not depleted by our strategy, and reciprocal NKT cell–DC activation has been described (59). We conclude that ISG15 is part of an innate route to promote the CTL response as an alternative or supplement to CD4⁺ T cell help (53). An earlier study reports that DC activation promoted by NK cell–derived IFN- γ could replace CD4⁺ T cell help in inducing a protective antitumor CD8⁺ T cell response (60) that supports this concept.

Our data tie together various independent observations on free ISG15 function that were primarily made in vitro and, even in human cells, into one concept that explains how free ISG15 can act as an alarmin and adjuvant to bridge innate and adaptive immunity. Our study relies on deliberate expression of ISG15, which has likely widened the window to observe this immune stimulatory function of ISG15 and its underlying mechanisms. By binding to USP18 and stabilizing it, intracellular free ISG15 promotes negative feedback on the type I IFN response in human, but not in mouse (7, 26). The question is whether this process would limit the application of free ISG15 as immune adjuvant in human. We show, in this study, that local and transient production of free ISG15 in the mouse skin is beneficial for the T cell response to therapeutic vaccination. In human, such a setting might be created as well, formulating free ISG15 and Ag either in pDNA or in protein form. In such vaccine-adjuvant settings, free ISG15 in proteinaceous form can only act extracellularly, and free ISG15

encoded by pDNA is expressed locally and transiently. For these reasons, the vaccine-adjuvant effect of free ISG15 may be reproducible in human.

Acknowledgments

We thank Astrid Bovens and the personnel of the experimental animal, flow cytometry, and genomics core facilities of the Netherlands Cancer Institute for expert assistance.

Disclosures

The authors have no financial conflicts of interest.

References

- Schneider, W. M., M. D. Chevillotte, and C. M. Rice. 2014. Interferon-stimulated genes: a complex web of host defenses. *Annu. Rev. Immunol.* 32: 513–545.
- Narasimhan, J., M. Wang, Z. Fu, J. M. Klein, A. L. Haas, and J. J. Kim. 2005. Crystal structure of the interferon-induced ubiquitin-like protein ISG15. *J. Biol. Chem.* 280: 27356–27365.
- Perng, Y. C., and D. J. Lenschow. 2018. ISG15 in antiviral immunity and beyond. *Nat. Rev. Microbiol.* 16: 423–439.
- Sampson, D. L., B. A. Fox, T. D. Yager, S. Bhide, S. Cermelli, L. C. McHugh, T. A. Seldon, R. A. Brandon, E. Sullivan, J. J. Zimmerman, et al. 2017. A four-biomarker blood signature discriminates systemic inflammation due to viral infection versus other etiologies. *Sci. Rep.* 7: 2914.
- Bogunovic, D., M. Byun, L. A. Durfee, A. Abhyankar, O. Sanal, D. Mansouri, S. Salem, I. Radovanovic, A. V. Grant, P. Adimi, et al. 2012. Mycobacterial disease and impaired IFN- γ immunity in humans with inherited ISG15 deficiency. *Science* 337: 1684–1688.
- Radoshevich, L., F. Impens, D. Ribet, J. J. Quereda, T. Nam Tham, M. A. Nahori, H. Bierre, O. Dussurget, J. Pizarro-Cerdá, K. P. Knobeloch, and P. Cossart. 2015. ISG15 counteracts *Listeria monocytogenes* infection. *eLife* 4: e06848.
- Dzimianski, J. V., F. E. M. Scholte, É. Bergeron, and S. D. Pegan. 2019. ISG15: it's complicated. *J. Mol. Biol.* 431: 4203–4216.
- Hermann, M., and D. Bogunovic. 2017. ISG15: in sickness and in health. *Trends Immunol.* 38: 79–93.
- Loeb, K. R., and A. L. Haas. 1992. The interferon-inducible 15-kDa ubiquitin homolog conjugates to intracellular proteins. *J. Biol. Chem.* 267: 7806–7813.
- Yuan, W., and R. M. Krug. 2001. Influenza B virus NS1 protein inhibits conjugation of the interferon (IFN)-induced ubiquitin-like ISG15 protein. *EMBO J.* 20: 362–371.
- Kim, K. I., N. V. Giannakopoulos, H. W. Virgin, and D. E. Zhang. 2004. Interferon-inducible ubiquitin E2, Ubc8, is a conjugating enzyme for protein ISGylation. *Mol. Cell. Biol.* 24: 9592–9600.
- Zhao, C., S. L. Beaudenon, M. L. Kelley, M. B. Waddell, W. Yuan, B. A. Schulman, J. M. Huibregtse, and R. M. Krug. 2004. The UbcH8 ubiquitin E2 enzyme is also the E2 enzyme for ISG15, an IFN- α /beta-induced ubiquitin-like protein. *Proc. Natl. Acad. Sci. USA* 101: 7578–7582.
- Dastur, A., S. Beaudenon, M. Kelley, R. M. Krug, and J. M. Huibregtse. 2006. Herc5, an interferon-induced HECT E3 enzyme, is required for conjugation of ISG15 in human cells. *J. Biol. Chem.* 281: 4334–4338.
- Ketscher, L., A. Basters, M. Prinz, and K. P. Knobeloch. 2012. mHERC6 is the essential ISG15 E3 ligase in the murine system. *Biochem. Biophys. Res. Commun.* 417: 135–140.
- Malakhov, M. P., O. A. Malakhova, K. I. Kim, K. J. Ritchie, and D. E. Zhang. 2002. UBP43 (USP18) specifically removes ISG15 from conjugated proteins. *J. Biol. Chem.* 277: 9976–9981.
- Durfee, L. A., N. Lyon, K. Seo, and J. M. Huibregtse. 2010. The ISG15 conjugation system broadly targets newly synthesized proteins: implications for the antiviral function of ISG15. *Mol. Cell* 38: 722–732.
- Liu, M., X. L. Li, and B. A. Hassel. 2003. Proteasomes modulate conjugation to the ubiquitin-like protein, ISG15. *J. Biol. Chem.* 278: 1594–1602.
- Zhang, X., D. Bogunovic, B. Payelle-Brogard, V. Francois-Newton, S. D. Spear, C. Yuan, S. Volpi, Z. Li, O. Sanal, D. Mansouri, et al. 2015. Human intracellular ISG15 prevents interferon- α / β over-amplification and auto-inflammation. *Nature* 517: 89–93.
- Fan, J. B., K. Arimoto, K. Motamedchaboki, M. Yan, D. A. Wolf, and D. E. Zhang. 2015. Identification and characterization of a novel ISG15-ubiquitin mixed chain and its role in regulating protein homeostasis. *Sci. Rep.* 5: 12704.
- Basters, A., K. P. Knobeloch, and G. Fritz. 2018. USP18 - a multifunctional component in the interferon response. *Biosci. Rep.* 38: BSR20180250.
- Ketscher, L., R. Hannß, D. J. Morales, A. Basters, S. Guerra, T. Goldmann, A. Hausmann, M. Prinz, R. Naumann, A. Pekosz, et al. 2015. Selective inactivation of USP18 isopeptidase activity in vivo enhances ISG15 conjugation and viral resistance. *Proc. Natl. Acad. Sci. USA* 112: 1577–1582.
- Rodriguez, M. R., K. Monte, L. B. Thackray, and D. J. Lenschow. 2014. ISG15 functions as an interferon-mediated antiviral effector early in the murine norovirus life cycle. *J. Virol.* 88: 9277–9286.
- Werneke, S. W., C. Schilte, A. Rohatgi, K. J. Monte, A. Michault, F. Arenzana-Seisdedos, D. L. Vanlandingham, S. Higgs, A. Fontanet, M. L. Albert, and

- D. J. Lenschow. 2011. ISG15 is critical in the control of Chikungunya virus infection independent of UbE1L mediated conjugation. *PLoS Pathog.* 7: e1002322.
24. Meuwissen, M. E., R. Schot, S. Buta, G. Oudesluijs, S. Tinschert, S. D. Speer, Z. Li, L. van Unen, D. Heijmans, T. Goldmann, et al. 2016. Human USP18 deficiency underlies type 1 interferonopathy leading to severe pseudo-TORCH syndrome. *J. Exp. Med.* 213: 1163–1174.
 25. Malakhova, O. A., K. I. Kim, J. K. Luo, W. Zou, K. G. Kumar, S. Y. Fuchs, K. Shuai, and D. E. Zhang. 2006. UBP43 is a novel regulator of interferon signaling independent of its ISG15 isopeptidase activity. *EMBO J.* 25: 2358–2367.
 26. Speer, S. D., Z. Li, S. Buta, B. Payelle-Brogard, L. Qian, F. Vigant, E. Rubino, T. J. Gardner, T. Wedeking, M. Hermann, et al. 2016. ISG15 deficiency and increased viral resistance in humans but not mice. *Nat. Commun.* 7: 11496.
 27. D’Cunha, J., S. Ramanujam, R. J. Wagner, P. L. Witt, E. Knight, Jr., and E. C. Borden. 1996. In vitro and in vivo secretion of human ISG15, an IFN-induced immunomodulatory cytokine. *J. Immunol.* 157: 4100–4108.
 28. Knight, E., Jr., and B. Cordova. 1991. IFN-induced 15-kDa protein is released from human lymphocytes and monocytes. *J. Immunol.* 146: 2280–2284.
 29. Padovan, E., L. Terracciano, U. Certa, B. Jacobs, A. Reschner, M. Bolli, G. C. Spagnoli, E. C. Borden, and M. Heberer. 2002. Interferon stimulated gene 15 constitutively produced by melanoma cells induces e-cadherin expression on human dendritic cells. *Cancer Res.* 62: 3453–3458.
 30. Taylor, J. L., J. D’Cunha, P. Tom, W. J. O’Brien, and E. C. Borden. 1996. Production of ISG-15, an interferon-inducible protein, in human corneal cells. *J. Interferon Cytokine Res.* 16: 937–940.
 31. Recht, M., E. C. Borden, and E. Knight, Jr. 1991. A human 15-kDa IFN-induced protein induces the secretion of IFN-gamma. *J. Immunol.* 147: 2617–2623.
 32. D’Cunha, J., E. Knight, Jr., A. L. Haas, R. L. Truitt, and E. C. Borden. 1996. Immunoregulatory properties of ISG15, an interferon-induced cytokine. *Proc. Natl. Acad. Sci. USA* 93: 211–215.
 33. Swaim, C. D., A. F. Scott, L. A. Canadeo, and J. M. Huijbregtse. 2017. Extracellular ISG15 signals cytokine secretion through the LFA-1 integrin receptor. *Mol. Cell* 68: 581–590.e5.
 34. Villarreal, D. O., M. C. Wise, R. J. Siefert, J. Yan, L. M. Wood, and D. B. Weiner. 2015. Ubiquitin-like molecule ISG15 acts as an immune adjuvant to enhance antigen-specific CD8 T-cell tumor immunity. *Mol. Ther.* 23: 1653–1662.
 35. Napolitano, A., A. G. van der Veen, M. Bunyan, A. Borg, D. Frith, S. Howell, S. Kjaer, A. Beling, A. P. Snijders, K. P. Knobloch, and E. M. Frickel. 2018. Cysteine-reactive free ISG15 generates IL-1 β -producing CD8 α + dendritic cells at the site of infection. *J. Immunol.* 201: 604–614.
 36. Osiak, A., O. Utermöhlen, S. Niendorf, I. Horak, and K. P. Knobloch. 2005. ISG15, an interferon-stimulated ubiquitin-like protein, is not essential for STAT1 signaling and responses against vesicular stomatitis and lymphocytic choriomeningitis virus. *Mol. Cell. Biol.* 25: 6338–6345.
 37. Oosterhuis, K., E. Aleyd, K. Vrijland, T. N. Schumacher, and J. B. Haanen. 2012. Rational design of DNA vaccines for the induction of human papillomavirus type 16 E6- and E7-specific cytotoxic T-cell responses. *Hum. Gene Ther.* 23: 1301–1312.
 38. Ahrends, T., N. Bąbala, Y. Xiao, H. Yagita, H. van Eenennaam, and J. Borst. 2016. CD27 agonism plus PD-1 blockade recapitulates CD4+ T-cell help in therapeutic anticancer vaccination. *Cancer Res.* 76: 2921–2931.
 39. Kasai, M., M. Iwamori, Y. Nagai, K. Okumura, and T. Tada. 1980. A glycolipid on the surface of mouse natural killer cells. *Eur. J. Immunol.* 10: 175–180.
 40. Love, M. I., W. Huber, and S. Anders. 2014. Moderated estimation of fold change and dispersion for RNA-seq data with DESeq2. *Genome Biol.* 15: 550.
 41. Ahrends, T., A. Spanjaard, B. Pilzecker, N. Bąbala, A. Bovens, Y. Xiao, H. Jacobs, and J. Borst. 2017. CD4+ T cell help confers a cytotoxic T cell effector program including coinhibitory receptor downregulation and increased tissue invasiveness. *Immunity* 47: 848–861.e5.
 42. Bąbala, N., A. Bovens, E. de Vries, V. Iglesias-Guimaraes, T. Ahrends, M. F. Krummel, J. Borst, and A. D. Bins. 2018. Subcellular localization of antigen in keratinocytes dictates delivery of CD4+ T-cell help for the CTL response upon therapeutic DNA vaccination into the skin. *Cancer Immunol. Res.* 6: 835–847.
 43. Chen, Y. L., W. L. Wu, C. W. Jang, Y. C. Yen, S. H. Wang, F. Y. Tsai, Y. Y. Shen, and Y. W. Chen. 2019. Interferon-stimulated gene 15 modulates cell migration by interacting with Rac1 and contributes to lymph node metastasis of oral squamous cell carcinoma cells. *Oncogene* 38: 4480–4495.
 44. Owhashi, M., Y. Taoka, K. Ishii, S. Nakazawa, H. Uemura, and H. Kambara. 2003. Identification of a ubiquitin family protein as a novel neutrophil chemotactic factor. *Biochem. Biophys. Res. Commun.* 309: 533–539.
 45. Ford, J. W., and D. W. McVicar. 2009. TREM and TREM-like receptors in inflammation and disease. *Curr. Opin. Immunol.* 21: 38–46.
 46. DiStasi, M. R., and K. Ley. 2009. Opening the flood-gates: how neutrophil-endothelial interactions regulate permeability. *Trends Immunol.* 30: 547–556.
 47. Monteleone, G., F. Pallone, and T. T. Macdonald. 2009. Interleukin-21 (IL-21)-mediated pathways in T cell-mediated disease. *Cytokine Growth Factor Rev.* 20: 185–191.
 48. Sa, S. M., P. A. Valdez, J. Wu, K. Jung, F. Zhong, L. Hall, I. Kasman, J. Winer, Z. Modrusan, D. M. Danilenko, and W. Ouyang. 2007. The effects of IL-20 subfamily cytokines on reconstituted human epidermis suggest potential roles in cutaneous innate defense and pathogenic adaptive immunity in psoriasis. *J. Immunol.* 178: 2229–2240.
 49. Maeda, S., M. Fujimoto, T. Matsushita, Y. Hamaguchi, K. Takehara, and M. Hasegawa. 2011. Inducible costimulator (ICOS) and ICOS ligand signaling has pivotal roles in skin wound healing via cytokine production. *Am. J. Pathol.* 179: 2360–2369.
 50. Yang, D., F. Wei, P. Tewary, O. M. Howard, and J. J. Oppenheim. 2013. Alarmin-induced cell migration. *Eur. J. Immunol.* 43: 1412–1418.
 51. Dos Santos, P. F., J. Van Weyenbergh, M. Delgobo, D. Oliveira Patricio, B. J. Ferguson, R. Guabiraba, T. Dierckx, S. M. Menezes, A. Báfica, and D. S. Mansur. 2018. ISG15-induced IL-10 is a novel anti-inflammatory myeloid axis disrupted during active tuberculosis. *J. Immunol.* 200: 1434–1442.
 52. Melief, C. J., T. van Hall, R. Arens, F. Ossendorp, and S. H. van der Burg. 2015. Therapeutic cancer vaccines. *J. Clin. Invest.* 125: 3401–3412.
 53. Borst, J., T. Ahrends, N. Bąbala, C. J. M. Melief, and W. Kastenmüller. 2018. CD4+ T cell help in cancer immunology and immunotherapy. *Nat. Rev. Immunol.* 18: 635–647.
 54. Verstrepen, B. E., A. D. Bins, C. S. Rollier, P. Mooij, G. Koopman, N. C. Sheppard, Q. Sattentau, R. Wagner, H. Wolf, T. N. Schumacher, et al. 2008. Improved HIV-1 specific T-cell responses by short-interval DNA tattooing as compared to intramuscular immunization in non-human primates. *Vaccine* 26: 3346–3351.
 55. Pampena, M. B., and E. M. Levy. 2015. Natural killer cells as helper cells in dendritic cell cancer vaccines. *Front. Immunol.* 6: 13.
 56. Buentke, E., L. C. Heffler, J. L. Wilson, R. P. Wallin, C. Löfman, B. J. Chambers, H. G. Ljunggren, and A. Scheynius. 2002. Natural killer and dendritic cell contact in lesional atopic dermatitis skin—Malassezia-influenced cell interaction. *J. Invest. Dermatol.* 119: 850–857.
 57. Ebert, L. M., S. Meuter, and B. Moser. 2006. Homing and function of human skin gammadelta T cells and NK cells: relevance for tumor surveillance. *J. Immunol.* 176: 4331–4336.
 58. Ferlazzo, G., and B. Morandi. 2014. Cross-talks between natural killer cells and distinct subsets of dendritic cells. *Front. Immunol.* 5: 159.
 59. Fujii, S., K. Shimizu, C. Smith, L. Bonifaz, and R. M. Steinman. 2003. Activation of natural killer T cells by alpha-galactosylceramide rapidly induces the full maturation of dendritic cells in vivo and thereby acts as an adjuvant for combined CD4 and CD8 T cell immunity to a coadministered protein. *J. Exp. Med.* 198: 267–279.
 60. Adam, C., S. King, T. Allgeier, H. Braumüller, C. Lüking, J. Mysliwicz, A. Kriegerkorte, D. H. Busch, M. Röcken, and R. Mocikat. 2005. DC-NK cell cross talk as a novel CD4+ T-cell-independent pathway for antitumor CTL induction. *Blood* 106: 338–344.
 61. Daczkowski, C. M., J. V. Dzimiński, J. R. Clasman, O. Goodwin, A. D. Mesecar, and S. D. Pegan. 2017. Structural insights into the interaction of coronavirus papain-like proteases and interferon-stimulated gene product 15 from different species. *J. Mol. Biol.* 429: 1661–1683.

Supplementary Table I

Differentially expressed genes in the skin of vaccinated mice
as a result of ISG15 expression

Gene ID	log2FoldChange	padj	Gene Name
ENSMUSG00000039269	6,421355349	0,005326	2300002M23Rik
ENSMUSG00000072845	3,844206463	3,55E-05	Tmprss11a
ENSMUSG00000044912	2,511317636	0,016638	Syt16
ENSMUSG00000040026	2,32587669	0,001152	Saa3
ENSMUSG00000021506	2,174140378	0,011725	Pitx1
ENSMUSG00000029236	2,091847464	0,02662	Nmu
ENSMUSG00000044737	2,08922121	0,017676	Klk14
ENSMUSG00000017211	1,975746608	4,87E-07	Gsdma2
ENSMUSG00000058260	1,915342333	4,05E-05	Serpina9
ENSMUSG00000027925	1,867673307	0,023204	Sprrr2j-ps
ENSMUSG00000028186	1,739612254	0,04765	Uox
ENSMUSG00000030577	1,668994159	0,037204	Cd22
ENSMUSG00000029379	1,655587861	1,46E-06	Cxcl3
ENSMUSG00000044430	1,6508633	0,013543	Klk12
ENSMUSG00000079451	1,63988091	0,035295	Tmprss11g
ENSMUSG00000001865	1,637234868	0,001073	Cpa3
ENSMUSG00000050195	1,632368984	0,035379	Scd4
ENSMUSG00000000901	1,628949124	9,47E-06	Mmp11
ENSMUSG00000096768	1,576203458	4,63E-05	Gm47283
ENSMUSG00000032323	1,539258596	0,012607	Cyp11a1
ENSMUSG00000074115	1,512978804	0,000561	Saa1
ENSMUSG00000051855	1,434705952	0,019959	Mest
ENSMUSG00000061068	1,407108853	0,001008	Mcpt4
ENSMUSG00000017737	1,372392231	5,53E-09	Mmp9
ENSMUSG00000022225	1,361556943	0,001236	Cma1
ENSMUSG00000042265	1,361131243	0,013839	Trem1
ENSMUSG00000052353	1,273436805	0,026572	Cemip
ENSMUSG00000064246	1,25132229	7,87E-08	Chil1
ENSMUSG00000026420	1,230974387	4,41E-08	Il24
ENSMUSG00000097768	1,189563542	0,047579	2310043M15Rik
ENSMUSG00000068011	1,179380588	0,044173	Mkrr2os
ENSMUSG00000033825	1,176918843	0,04009	Tpsb2
ENSMUSG00000029378	1,144666384	1,21E-05	Areg
ENSMUSG00000029380	1,136749898	0,001806	Cxcl1
ENSMUSG00000017002	1,130988437	0,003986	Slpi
ENSMUSG00000045362	1,129862878	0,009172	Tnfrsf26
ENSMUSG00000030142	1,125860658	0,042927	Clec4e
ENSMUSG00000023992	1,121405722	0,02662	Trem2
ENSMUSG00000013974	1,103984962	0,028177	Mcemp1
ENSMUSG00000094733	1,062430168	0,044858	Csta3
ENSMUSG00000032487	1,052593035	1,23E-06	Ptgs2
ENSMUSG00000032291	1,046250757	0,006485	Crabp1

ENSMUSG00000021384	1,035594962	0,046037	Susd3
ENSMUSG00000039519	1,025980488	1,97E-05	Cyp7b1
ENSMUSG00000078122	1,006458615	0,020007	F630028O10Rik
ENSMUSG00000028111	0,992811335	3,49E-16	Ctsk
ENSMUSG00000068748	0,984109227	0,007195	Ptprz1
ENSMUSG00000027737	0,979615947	0,000996	Slc7a11
ENSMUSG00000046223	0,978054451	0,031742	Plaur
ENSMUSG00000092500	0,969180706	0,0288	Gm20400
ENSMUSG00000078190	0,951019947	0,000164	Dnm3os
ENSMUSG00000042286	0,943393005	1,31E-05	Stab1
ENSMUSG00000054555	0,937511893	0,001567	Adam12
ENSMUSG00000026837	0,927487068	5,11E-06	Col5a1
ENSMUSG00000008136	0,925099842	0,03089	Fhl2
ENSMUSG00000028364	0,916292337	0,004361	Tnc
ENSMUSG00000030351	0,912726326	1,08E-07	Tspan11
ENSMUSG00000028459	0,910521019	7,87E-08	Cd72
ENSMUSG00000046733	0,909557771	0,028841	Gprc5a
ENSMUSG00000030693	0,899283575	1,68E-05	Klk10
ENSMUSG00000097779	0,885012666	0,013543	4833407H14Rik
ENSMUSG00000030745	0,882571415	0,017805	Il21r
ENSMUSG00000097636	0,879235419	0,003014	Mirt1
ENSMUSG00000020205	0,87624149	7,11E-11	Phlda1
ENSMUSG00000034205	0,874638646	0,000398	Loxl2
ENSMUSG00000094686	0,867455094	0,041188	Ccl21a
ENSMUSG00000029163	0,864265825	0,000477	Emilin1
ENSMUSG00000027408	0,860898724	6,54E-05	Cpxm1
ENSMUSG0000001506	0,857352078	5,34E-05	Col1a1
ENSMUSG00000054675	0,83153686	0,000424	Tmem119
ENSMUSG00000024409	0,824540193	3,51E-05	Psors1c2
ENSMUSG00000037411	0,819904283	6,96E-09	Serpine1
ENSMUSG00000007805	0,792848143	0,009343	Twist2
ENSMUSG00000031673	0,788928644	0,019852	Cdh11
ENSMUSG00000026288	0,784145179	0,011272	Inpp5d
ENSMUSG00000004709	0,76642552	0,041403	Cd244a
ENSMUSG00000023411	0,765255331	2,42E-06	Nfatc4
ENSMUSG00000027314	0,763145654	0,018071	Dll4
ENSMUSG00000031595	0,761139219	0,025933	Pdgfrl
ENSMUSG00000022094	0,743639187	0,017883	Slc39a14
ENSMUSG00000026535	0,743358925	8,57E-06	Ifi202b
ENSMUSG00000040751	0,743351542	0,009406	Lat2
ENSMUSG00000047810	0,735006652	0,000185	Ccdc88b
ENSMUSG00000007207	0,718790475	0,016684	Stx1a
ENSMUSG00000038642	0,708982277	0,017676	Ctss
ENSMUSG00000001555	0,703392704	0,025798	Fkbp10
ENSMUSG00000009633	0,702400517	0,006786	G0s2
ENSMUSG00000015468	0,696335935	0,000933	Notch4
ENSMUSG00000070691	0,695538637	0,010694	Runx3
ENSMUSG00000064080	0,695255844	0,002658	Fbln2

ENSMUSG0000006519	0,688646873	0,042697	Cyba
ENSMUSG00000054342	0,682809703	0,010849	Kcnn4
ENSMUSG00000060572	0,677834947	0,00266	Mfap2
ENSMUSG00000023913	0,676818019	1,24E-05	Pla2g7
ENSMUSG00000042244	0,667243516	0,027383	Pglyrp3
ENSMUSG00000048163	0,665512979	0,028952	Selplg
ENSMUSG00000028597	0,665063254	0,018066	Gpx7
ENSMUSG00000030789	0,662307847	0,037188	Itgax
ENSMUSG00000024180	0,660586055	0,044305	Tmem8
ENSMUSG00000044165	0,657344013	0,00239	Bcl2l15
ENSMUSG00000039883	0,65204413	0,008785	Lrrc17
ENSMUSG00000045027	0,651976441	0,003017	Prss22
ENSMUSG00000026043	0,647164999	0,045461	Col3a1
ENSMUSG00000030748	0,637886497	0,006786	Il4ra
ENSMUSG00000036446	0,634706184	0,001367	Lum
ENSMUSG00000031375	0,632640341	3,57E-05	Bgn
ENSMUSG00000026180	0,621601842	0,028617	Cxcr2
ENSMUSG00000032369	0,620308026	0,017997	Plscr1
ENSMUSG00000026042	0,616621554	0,000409	Col5a2
ENSMUSG00000031169	0,610793592	0,02662	Porcn
ENSMUSG00000030218	0,610575628	0,000904	Mgp
ENSMUSG00000024397	0,61042352	0,049939	Aif1
ENSMUSG00000031558	0,606473434	0,030161	Slit2
ENSMUSG00000084910	0,60206019	0,047274	C630043F03Rik
ENSMUSG00000032997	0,601949237	0,036126	Chpf
ENSMUSG00000044258	0,601130649	0,006964	Ctla2a
ENSMUSG00000003541	0,598110369	0,00119	Ier3
ENSMUSG00000036862	0,597555706	0,012574	Dchs1
ENSMUSG00000041378	0,595497938	0,027501	Cldn5
ENSMUSG00000056515	0,593738783	0,007195	Rab31
ENSMUSG00000056413	0,590904742	0,009027	Adap1
ENSMUSG00000031486	0,579652656	0,036215	Adgra2
ENSMUSG00000057751	0,572054022	0,000344	Megf6
ENSMUSG00000031827	0,565248704	0,033137	Cotl1
ENSMUSG00000036334	0,549644551	0,003294	Igsf10
ENSMUSG00000038074	0,546506509	0,038241	Fkbp14
ENSMUSG00000022098	0,542350591	0,002903	Bmp1
ENSMUSG00000021411	0,537036492	0,000849	Pxdc1
ENSMUSG00000003573	0,533829202	0,023204	Homer3
ENSMUSG00000002732	0,531713566	0,009343	Fkbp7
ENSMUSG00000021608	0,527454653	0,0424	Lpcat1
ENSMUSG00000024846	0,526435052	0,006975	Cst6
ENSMUSG00000026360	0,523506164	2,61E-05	Rgs2
ENSMUSG00000054364	0,519814861	0,001236	Rhob
ENSMUSG00000029816	0,505545896	0,010925	Gpnmb
ENSMUSG00000020186	0,498583245	0,044425	Csrp2
ENSMUSG00000000957	0,493436807	0,0014	Mmp14
ENSMUSG00000048677	0,492804241	0,017174	Tpcn2

ENSMUSG00000021556	0,492089142	0,038604	Golm1
ENSMUSG00000031740	0,489135828	0,019289	Mmp2
ENSMUSG00000031538	0,488184532	0,002843	Plat
ENSMUSG00000027859	0,487603364	0,038372	Ngf
ENSMUSG00000026921	0,485364974	0,008966	Egfl7
ENSMUSG00000056708	0,483729339	0,000321	Ier5
ENSMUSG00000030123	0,48008909	0,015692	Plxnd1
ENSMUSG00000048126	0,477972234	0,012481	Col6a3
ENSMUSG00000020241	0,471947209	0,000106	Col6a2
ENSMUSG00000021477	0,471392902	0,028617	Ctsl
ENSMUSG00000090946	0,470998508	0,029062	Ccdc71l
ENSMUSG00000037580	0,469994632	0,02335	Gch1
ENSMUSG00000028073	0,465232265	0,018246	Pear1
ENSMUSG00000032068	0,458648339	0,012456	Plet1
ENSMUSG00000026479	0,455300425	0,009714	Lamc2
ENSMUSG00000034675	0,450444109	0,022163	Dbn1
ENSMUSG00000021451	0,447707589	0,002435	Sema4d
ENSMUSG00000029999	0,438432715	0,000155	Tgfa
ENSMUSG00000025283	0,429225247	0,000236	Sat1
ENSMUSG00000022969	0,427546092	0,013556	Il10rb
ENSMUSG00000090084	0,427482318	0,032848	Srpx
ENSMUSG00000053175	0,423191385	0,034772	Bcl3
ENSMUSG00000022048	0,410823974	0,049646	Dpysl2
ENSMUSG00000070436	0,40701252	0,043409	Serpinh1
ENSMUSG00000021262	0,402586038	0,028034	Evl
ENSMUSG00000000732	0,39628807	0,026659	Icosl
ENSMUSG00000020092	0,390723546	0,019107	Pald1
ENSMUSG00000021904	0,379538798	0,03459	Sema3g
ENSMUSG00000005413	0,377936385	0,000331	Hmox1
ENSMUSG00000021186	0,372710697	0,022456	Fbln5
ENSMUSG00000001119	0,366117264	0,012481	Col6a1
ENSMUSG00000021806	0,364328665	0,014784	Nid2
ENSMUSG00000028059	0,345570608	0,028617	Arhgef2
ENSMUSG00000027333	0,344660665	0,018004	Smox
ENSMUSG00000023905	0,331284452	0,002013	Tnfrsf12a
ENSMUSG00000028339	0,325944043	0,007195	Col15a1
ENSMUSG00000052423	0,320551792	0,031819	B4galt3
ENSMUSG00000031765	0,307536492	0,02839	Mt1
ENSMUSG00000001435	0,297194581	0,026659	Col18a1
ENSMUSG00000092341	0,200623114	0,044866	Malat1
ENSMUSG00000029472	-0,193548385	0,044449	Anapc5
ENSMUSG00000006373	-0,241786861	0,023945	Pgrmc1
ENSMUSG00000015961	-0,242108065	0,037402	Adss
ENSMUSG00000024900	-0,253786214	0,048846	Cpt1a
ENSMUSG00000057614	-0,260069073	0,048846	Gnai1
ENSMUSG00000020023	-0,26142792	0,017805	Tmcc3
ENSMUSG00000028565	-0,26699044	0,044858	Nfia
ENSMUSG00000025745	-0,268168207	0,00643	Hadha

ENSMUSG00000018796	-0,268565289	0,014425	Acsl1
ENSMUSG00000072812	-0,273609147	0,00985	Ahnak2
ENSMUSG00000028127	-0,275481842	0,001809	Abcd3
ENSMUSG00000027809	-0,276990141	0,038547	Etfdh
ENSMUSG00000027680	-0,277587003	0,034732	Fxr1
ENSMUSG00000025404	-0,278677092	0,041881	R3hdm2
ENSMUSG00000030852	-0,283736049	0,000852	Tacc2
ENSMUSG00000063077	-0,287451796	0,023177	Kif1b
ENSMUSG00000030557	-0,289877361	0,020989	Mef2a
ENSMUSG00000053768	-0,291892519	0,008058	Chchd3
ENSMUSG00000039428	-0,293158079	0,035295	Tmem135
ENSMUSG00000002010	-0,297894338	0,044858	Idh3g
ENSMUSG00000038236	-0,299688031	0,008966	Hoxa7
ENSMUSG00000015619	-0,304886006	0,00661	Gata3
ENSMUSG00000021950	-0,306726081	0,009343	Anxa8
ENSMUSG00000027187	-0,310315845	0,045225	Cat
ENSMUSG00000021094	-0,314378912	0,049646	Dhrs7
ENSMUSG00000053898	-0,316388854	0,021161	Ech1
ENSMUSG00000030739	-0,319210582	0,027383	Myh14
ENSMUSG00000024981	-0,321050725	0,009343	Acsl5
ENSMUSG00000031782	-0,325497856	0,020007	Coq9
ENSMUSG00000055320	-0,328629254	0,025766	Tead1
ENSMUSG00000021236	-0,332335507	0,016638	Entpd5
ENSMUSG00000046324	-0,336095745	0,01569	Ermp1
ENSMUSG00000058022	-0,34041433	0,01436	Adtrp
ENSMUSG00000032047	-0,343927546	0,025568	Acat1
ENSMUSG00000056602	-0,344205647	0,017883	Fry
ENSMUSG00000001211	-0,346533282	0,013247	Agpat3
ENSMUSG00000047454	-0,347076342	0,021864	Gphn
ENSMUSG00000031708	-0,348800883	0,001262	Tecr
ENSMUSG00000041548	-0,351712318	0,016008	Hspb8
ENSMUSG00000064368	-0,355352781	0,019289	mt-Nd6
ENSMUSG00000064337	-0,361462027	1,03E-05	mt-Rnr1
ENSMUSG00000028496	-0,362751254	0,011593	Mllt3
ENSMUSG00000024782	-0,366781921	0,003837	Ak3
ENSMUSG00000048490	-0,371820467	0,011272	Nrip1
ENSMUSG00000062929	-0,385087506	0,002869	Cfl2
ENSMUSG00000030987	-0,385189143	0,006013	Stim1
ENSMUSG00000026827	-0,398724321	0,02958	Gpd2
ENSMUSG00000032281	-0,39929544	0,001815	Acsbg1
ENSMUSG00000029432	-0,39976452	0,000547	Nipsnap2
ENSMUSG00000021417	-0,403696465	0,027486	Eci2
ENSMUSG00000030077	-0,405742681	0,001723	Chl1
ENSMUSG00000003949	-0,409888537	0,046844	Hlf
ENSMUSG00000023861	-0,412933592	0,013078	Mpc1
ENSMUSG00000037710	-0,417524195	0,017676	Cisd1
ENSMUSG00000027288	-0,422725161	0,006555	Zfp106
ENSMUSG00000036960	-0,43604616	0,003977	Clca2

ENSMUSG00000055053	-0,436998777	0,029941	Nfic
ENSMUSG00000004558	-0,45689405	0,006142	Ndrp2
ENSMUSG00000019883	-0,461691682	0,01875	Echdc1
ENSMUSG00000037736	-0,463777336	0,049646	Limch1
ENSMUSG00000064370	-0,466844183	0,000746	mt-Cytb
ENSMUSG00000026463	-0,467203537	0,004671	Atp2b4
ENSMUSG00000026778	-0,468524785	0,027014	Prkcq
ENSMUSG00000027868	-0,46991702	0,017883	Tbx15
ENSMUSG00000054893	-0,477581751	0,049646	Zfp667
ENSMUSG00000024206	-0,482246286	0,019466	Rfx2
ENSMUSG00000031245	-0,486235288	0,003962	Hmgn5
ENSMUSG00000038936	-0,487598185	0,022506	Sccpdh
ENSMUSG00000037989	-0,48804183	0,016008	Wnk2
ENSMUSG00000027488	-0,489334492	0,028518	Snta1
ENSMUSG00000038886	-0,491774041	0,041477	Man2a2
ENSMUSG00000042613	-0,495103831	0,009658	Pbxip1
ENSMUSG00000028519	-0,497306649	0,044305	Dab1
ENSMUSG00000026220	-0,501001009	0,012941	Slc16a14
ENSMUSG00000026600	-0,502368534	0,026028	Soat1
ENSMUSG00000072949	-0,509263528	0,022506	Acot1
ENSMUSG00000032262	-0,510585521	0,01279	Elovl4
ENSMUSG00000000125	-0,5167588	7,46E-05	Wnt3
ENSMUSG00000064341	-0,529109096	1,18E-06	mt-Nd1
ENSMUSG00000064351	-0,529300649	8,95E-09	mt-Co1
ENSMUSG00000028949	-0,530034266	0,041147	Smarcd3
ENSMUSG00000060548	-0,533790353	0,009275	Tnfrsf19
ENSMUSG00000021238	-0,544523716	0,003017	Aldh6a1
ENSMUSG00000021573	-0,548832339	0,045491	Tppp
ENSMUSG00000089960	-0,55165506	0,018001	Ugt1a1
ENSMUSG00000037762	-0,554872992	0,008966	Slc16a9
ENSMUSG00000055980	-0,560541977	0,024253	Irs1
ENSMUSG00000025997	-0,56536026	0,015692	Ikzf2
ENSMUSG00000078598	-0,570554942	0,028034	Skint5
ENSMUSG00000039345	-0,572008766	0,020536	Mettl22
ENSMUSG00000008206	-0,575406058	0,022456	Cers4
ENSMUSG00000047045	-0,576757631	0,010925	Tmem164
ENSMUSG00000090637	-0,590952119	0,02958	Gm6189
ENSMUSG00000040170	-0,599003573	0,046292	Fmo2
ENSMUSG00000000876	-0,599130019	0,004255	Pxmp4
ENSMUSG00000031633	-0,612619486	0,002748	Slc25a4
ENSMUSG00000027380	-0,613930713	0,001231	Acoxl
ENSMUSG00000026853	-0,617982847	0,023591	Crat
ENSMUSG00000030695	-0,618439626	8,3E-11	Aldoa
ENSMUSG00000064363	-0,62840062	7,48E-06	mt-Nd4
ENSMUSG00000029120	-0,633416651	0,023204	Ppp2r2c
ENSMUSG00000027869	-0,668270631	0,023204	Hsd3b6
ENSMUSG00000030303	-0,681194025	0,022456	Far2
ENSMUSG00000028464	-0,68198156	0,002555	Tpm2

ENSMUSG00000023927	-0,684888375	0,01279	Satb1
ENSMUSG00000028132	-0,693137661	0,026659	Tmem56
ENSMUSG00000033849	-0,694876205	0,030355	B3galt2
ENSMUSG00000019528	-0,724647064	0,008733	Gyg
ENSMUSG00000074093	-0,733846544	0,019959	Svip
ENSMUSG00000099889	-0,73663846	0,00145	Mrgprb11-ps
ENSMUSG00000031137	-0,739818997	0,008062	Fgf13
ENSMUSG00000031220	-0,740176115	0,035722	Awat2
ENSMUSG00000064345	-0,743999773	1,53E-11	mt-Nd2
ENSMUSG00000033533	-0,746675783	0,014924	Acsm1
ENSMUSG00000024924	-0,750252777	2,23E-05	Vldlr
ENSMUSG00000064367	-0,774353597	2,63E-08	mt-Nd5
ENSMUSG00000041220	-0,797321125	0,007141	Elovl6
ENSMUSG00000028427	-0,798640475	0,048143	Aqp7
ENSMUSG00000030249	-0,803095142	0,004255	Abcc9
ENSMUSG00000070546	-0,821627616	9,98E-05	Mrgprb3
ENSMUSG00000055493	-0,826835731	0,00039	Epm2a
ENSMUSG00000064356	-0,827235123	4,48E-05	mt-Atp8
ENSMUSG00000030319	-0,832019124	1,46E-06	Cand2
ENSMUSG00000026489	-0,841355991	0,028617	Coq8a
ENSMUSG00000068699	-0,847273462	0,019466	Flnc
ENSMUSG00000029095	-0,862328997	0,0011	Ablim2
ENSMUSG00000040254	-0,862509969	0,013902	Sema3d
ENSMUSG00000074661	-0,874889712	0,020011	
ENSMUSG00000096606	-0,875147368	2,64E-05	Tpbgl
ENSMUSG00000026817	-0,891470239	1,04E-08	Ak1
ENSMUSG00000033400	-0,90250612	9,42E-10	Agl
ENSMUSG00000051107	-0,906496584	0,024238	
ENSMUSG00000018566	-0,925614044	0,016284	Slc2a4
ENSMUSG00000051910	-0,93381366	1,43E-07	Sox6
ENSMUSG00000042828	-0,948850074	4,77E-07	Trim72
ENSMUSG00000000253	-0,966419624	0,004997	Gmpr
ENSMUSG00000023336	-0,981438513	0,003544	Wfdc1
ENSMUSG00000032366	-0,998969566	1,59E-11	Tpm1
ENSMUSG00000005583	-1,003587987	2,14E-08	Mef2c
ENSMUSG00000058975	-1,040690018	0,036197	Kcnc1
ENSMUSG00000011305	-1,041094361	0,044305	Plin5
ENSMUSG00000027559	-1,053558829	0,000102	Car3
ENSMUSG00000049241	-1,059981658	0,028017	Hcar1
ENSMUSG00000021768	-1,082206788	0,026659	Dusp13
ENSMUSG00000028518	-1,096110209	1,43E-09	Prkaa2
ENSMUSG00000041688	-1,129650761	0,000253	Amot
ENSMUSG00000007097	-1,129863757	0,003248	Atp1a2
ENSMUSG000000101655	-1,137419331	0,036351	2310040G24Rik
ENSMUSG00000026207	-1,143590716	1,55E-06	Speg
ENSMUSG00000025932	-1,150054933	0,028617	Eya1
ENSMUSG00000027499	-1,163557056	1,93E-14	Pkia
ENSMUSG00000038132	-1,170058344	0,002514	Rbm24

ENSMUSG00000028116	-1,181456995	0,034772	Myoz2
ENSMUSG00000041889	-1,18277952	0,004361	Shisa4
ENSMUSG00000038201	-1,19282871	0,022506	Kcna7
ENSMUSG00000023959	-1,202327634	3,88E-06	Clic5
ENSMUSG00000030554	-1,204849968	1,22E-15	Synm
ENSMUSG00000064179	-1,209158683	5,69E-05	Tnnt1
ENSMUSG00000026208	-1,224641433	2,18E-05	Des
ENSMUSG00000074218	-1,22488414	0,000122	Cox7a1
ENSMUSG00000039103	-1,243750176	1,1E-05	Nexn
ENSMUSG00000002007	-1,25222249	0,019687	Srpk3
ENSMUSG00000026418	-1,258722643	2,34E-05	Tnni1
ENSMUSG00000021061	-1,264796253	9,25E-06	Sptb
ENSMUSG00000071342	-1,274979458	0,023204	Lsmem1
ENSMUSG00000028017	-1,290649963	8,82E-05	Egf
ENSMUSG00000032355	-1,297853511	7,39E-09	Mlip
ENSMUSG00000074001	-1,301923353	0,001735	Klhl40
ENSMUSG00000038663	-1,318298696	0,000155	Fsd2
ENSMUSG00000031519	-1,321717341	0,028928	Asb5
ENSMUSG00000029158	-1,32718159	0,000285	Yipf7
ENSMUSG00000038763	-1,329864247	0,021379	Alpk3
ENSMUSG00000020216	-1,341752226	2,53E-05	Jsrp1
ENSMUSG00000030996	-1,34221123	8,06E-05	Art1
ENSMUSG00000042451	-1,348899142	1,41E-05	Mybph
ENSMUSG00000031636	-1,377069591	4,73E-06	Pdlim3
ENSMUSG00000032942	-1,381889583	0,000512	Ucp3
ENSMUSG00000030621	-1,382871825	0,00015	Me3
ENSMUSG00000031791	-1,387434355	1,94E-13	Tmem38a
ENSMUSG00000040118	-1,394529764	5,38E-17	Cacna2d1
ENSMUSG00000044086	-1,420164486	0,020121	Lmod3
ENSMUSG00000035296	-1,426449596	0,000128	Sgcg
ENSMUSG00000030317	-1,435988586	0,012675	Timp4
ENSMUSG00000071317	-1,442576183	0,001153	Bves
ENSMUSG00000021456	-1,447923144	0,019402	Fbp2
ENSMUSG00000002500	-1,488508331	1,97E-06	Rpl3l
ENSMUSG00000031382	-1,502831205	1,92E-07	Asb11
ENSMUSG00000021373	-1,515664838	4,29E-08	Cap2
ENSMUSG00000049134	-1,523446701	3,78E-08	Nrap
ENSMUSG00000085779	-1,535823222	0,01229	Atcayos
ENSMUSG00000028328	-1,542508518	8,93E-06	Tmod1
ENSMUSG00000079588	-1,55942896	3,38E-06	Tmem182
ENSMUSG00000028023	-1,56271553	0,047122	Pitx2
ENSMUSG00000005628	-1,569207407	2,23E-21	Tmod4
ENSMUSG00000040666	-1,570867923	5,45E-14	Sh3bgr
ENSMUSG00000028348	-1,585836807	3,96E-06	Cavin4
ENSMUSG00000039376	-1,604952098	3,29E-06	Synpo2l
ENSMUSG00000022215	-1,611773935	9,32E-06	Fitm1
ENSMUSG00000072720	-1,612187687	1,86E-05	Myo18b
ENSMUSG00000030785	-1,62777329	5,5E-11	Cox6a2

ENSMUSG00000026308	-1,632748512	9,62E-05	Klhl30
ENSMUSG00000034055	-1,644588085	1,96E-05	Phka1
ENSMUSG00000031097	-1,650858113	2,86E-14	Tnni2
ENSMUSG00000021798	-1,652483606	4,06E-07	Ldb3
ENSMUSG00000028396	-1,652489313	1,97E-05	2310002L09Rik
ENSMUSG00000038204	-1,657051279	0,012185	Asb10
ENSMUSG00000020061	-1,663105587	0,012185	Mybpc1
ENSMUSG00000028033	-1,666583607	0,000423	Kcnq5
ENSMUSG00000001508	-1,675379381	3,97E-11	Sgca
ENSMUSG00000024049	-1,684419612	4,29E-08	Myom1
ENSMUSG00000017817	-1,6889505	4,23E-17	Jph2
ENSMUSG00000062077	-1,697412839	1,17E-08	Trim54
ENSMUSG00000017300	-1,698454891	3,49E-16	Tnnc2
ENSMUSG00000028278	-1,73939365	3,97E-11	Rragd
ENSMUSG00000021579	-1,741918728	1,18E-06	Lrrc14b
ENSMUSG00000027961	-1,746069452	2,45E-07	Lrrc39
ENSMUSG00000038170	-1,764247944	1,32E-23	Pde4dip
ENSMUSG00000038239	-1,774724073	6,58E-09	Hrc
ENSMUSG00000038526	-1,785353485	0,044351	Car14
ENSMUSG00000051367	-1,801694432	1,06E-05	Six1
ENSMUSG00000038403	-1,804444731	4,57E-16	Hjv
ENSMUSG00000087090	-1,804536908	7,99E-06	Nctc1
ENSMUSG00000031461	-1,819736453	0,002507	Myom2
ENSMUSG00000055027	-1,830468665	7,5E-08	Smyd1
ENSMUSG00000078815	-1,838460143	1,75E-07	Cacng6
ENSMUSG00000042686	-1,848615371	3,54E-19	Jph1
ENSMUSG00000042476	-1,852478985	3,96E-06	Abcb4
ENSMUSG00000016349	-1,854229758	2,62E-10	Eef1a2
ENSMUSG00000031543	-1,882346948	3,27E-14	Ank1
ENSMUSG00000030672	-1,883558833	2,23E-18	Mylpf
ENSMUSG00000021898	-1,885219399	7,64E-06	Asb14
ENSMUSG00000020067	-1,907124693	1,57E-07	Mypn
ENSMUSG00000061723	-1,909208913	4,42E-18	Tnnt3
ENSMUSG00000028584	-1,912405789	0,028928	Lrrc38
ENSMUSG00000079055	-1,916534129	1,46E-06	Slc8a3
ENSMUSG00000055489	-1,93982409	7,11E-11	Ano5
ENSMUSG00000046345	-1,940257305	0,01478	Smco1
ENSMUSG00000010492	-1,941429424	2,42E-06	Uckl1os
ENSMUSG00000025537	-1,942263744	1,73E-09	Phkg1
ENSMUSG00000047746	-1,973396751	7,93E-17	Fbxo40
ENSMUSG00000040705	-1,974530684	0,000561	A930016O22Rik
ENSMUSG00000043795	-1,975964063	1,66E-17	Prr33
ENSMUSG00000061816	-1,982851068	2,25E-19	Myl1
ENSMUSG00000027887	-1,994066224	3,54E-19	Sypl2
ENSMUSG00000030592	-2,075631685	2,35E-19	Ryr1
ENSMUSG00000027470	-2,086872951	3,54E-19	Mylk2
ENSMUSG00000001027	-2,09492891	1,75E-11	Scn4a
ENSMUSG00000051980	-2,099926356	0,016674	Casr

ENSMUSG00000068697	-2,123031719	5,42E-18	Myoz1
ENSMUSG00000007122	-2,138514335	3,51E-26	Casq1
ENSMUSG00000026407	-2,153452352	9,58E-19	Cacna1s
ENSMUSG00000067081	-2,154300002	0,003437	Asb18
ENSMUSG00000047419	-2,208551938	2,48E-21	Cmya5
ENSMUSG00000026950	-2,256764963	2,5E-17	Neb
ENSMUSG00000029862	-2,336834803	7,84E-14	Clcn1
ENSMUSG00000042717	-2,362193164	8,01E-13	Ppp1r3a
ENSMUSG00000031204	-2,462419663	7,88E-05	Asb12
ENSMUSG00000030730	-2,486898441	1,5E-25	Atp2a1
ENSMUSG00000045776	-2,631371351	0,021183	Lrtm1
ENSMUSG00000063821	-2,83814977	0,000815	Dupd1
ENSMUSG00000038670	-2,864362671	6,79E-09	Mybpc2
ENSMUSG00000079278	-2,870029933	6,97E-32	Tmem233
ENSMUSG00000044951	-3,074864749	3,58E-12	Mylk4
ENSMUSG00000026100	-3,079475819	0,000128	Mstn
ENSMUSG00000047343	-3,374676566	0,007361	Mettl21c
ENSMUSG00000026173	-4,029956325	3,94E-11	Plcd4